Geol. Mag. **156** (*3*), *2019, pp. 547–571* © *Cambridge University Press 2017*
doi:10.1017/S0016756817000978

Provenance and tectonic setting of the Upper Palaeozoic sandstones in western Inner Mongolia (the Shalazhashan and Solonker belts), China: insights from detrital zircon U–Pb ages and Hf isotopes

GUANZHONG SHI*‡, GUANGZENG SONG§, HUA WANG*‡†, CHUANYAN HUANG*‡ & BEN LI¶

*Key Laboratory of Tectonics and Petroleum Resources, Ministry of Education, China University of Geosciences, Wuhan 430074, China
‡Faculty of Earth Resources, China University of Geosciences, Wuhan 430074, China
§School of Resources and Environment, University of Ji'nan, Ji'nan 250022, China
¶Institute of Petroleum Exploration and Development, PetroChina Huabei Oilfield Company, Cangzhou 062552, China

(*Received* 6 July 2017; *accepted* 10 October 2017; *first published online* 14 December 2017)

Abstract – The Solonker and Shalazhashan belts are hotly debated tectonic units of the Central Asian Orogenic Belt (CAOB), because they may either represent a Permian or Triassic suture zone of the CAOB, or a rifting zone overprinted on an Early Palaeozoic orogen. Provenance analysis of the Upper Palaeozoic sandstones in these belts may provide useful constraints on this issue. This study collected six sandstone samples from three study areas: the Mandula area of the Solonker Belt, the Quagan Qulu area of the Shalazhashan Belt but close to the Alxa block, and the Enger Us area of the Shalazhashan Belt, for framework petrography, zircon morphology, U–Pb and Lu–Hf isotopic analyses. Framework petrography reveals that the Mandula and Enger Us area samples contain high proportions of volcanic fragments, whereas the samples from the Quagan Qulu area include not only volcanic fragments but also significant amounts of biotite and muscovite. The detrital zircons of the Mandula area and the Enger Us area yield two main age groups: (i) 260–330 Ma, with dominant $\varepsilon_{Hf}(t)$ values of –5 to +12; and (ii) 420–550 Ma, with dominant $\varepsilon_{Hf}(t)$ values of –9 to +9, suggesting that Early Palaeozoic arc-related magmatic rocks and Late Palaeozoic syn-depositional volcanic rocks are the main source rocks. The detrital zircons of the Quagan Qulu area have one main age group of 420–500 Ma and some grains of 0.9–1.1 Ga, 1.4–1.5 Ga, 1.8–1.9 Ga and ~ 2.5 Ga, which derive from the northern margin of the Alxa block. The lithological and fossil assemblages of the Upper Palaeozoic sandstones suggest shallow-marine to deep-water depositional environments and a northward-deepening transition. Based on the zircon spectra, sedimentary environment analysis and previous studies, we argue that the Solonker Belt and the Shalazhashan Belt of the CAOB are in extensional basins of a fore-arc or rifting setting.

Keywords: provenance analysis, detrital zircon, U–Pb ages, Amushan Formation, CAOB

1. Introduction

The Central Asian Orogenic Belt (CAOB) is a giant accretionary orogenic belt between the Siberian Craton and the North China–Tarim cratons (Sengör, Natal'in & Burtman, 1993; Jahn *et al.* 2004; Windley *et al.* 2007; Xiao *et al.* 2009, 2010; Kröner *et al.* 2014). It was built up by multiple subduction/accretionary processes along with the closure of the Palaeo-Asian Ocean and involved a variety of tectonic units such as Precambrian microcontinents, ancient island arcs, fragments of oceanic islands and seamounts, accretionary complexes and passive continental margins (Mossakovsky *et al.* 1993; Sengör, Natal'in & Burtman, 1993; Jahn, 2004; Windley *et al.* 2007; Xiao *et al.* 2010, 2015). However, the tectonic processes concerning the last-stage evolution of the Palaeo-Asian Ocean and the formation of the CAOB have been hotly debated (Wang & Liu, 1986; Tang, 1990; Sengör, Natal'in & Burtman, 1993; Xiao *et al.* 2003, 2009; Windley *et al.* 2007; Choulet *et al.* 2013). Suggestions for the timing of the final closure of the Palaeo-Asian Ocean range from Late Devonian to Triassic (Xiao *et al.* 2003; Charvet *et al.* 2011; Xu *et al.* 2013; Eizenhöfer *et al.* 2014, 2015*a*,*b*; Shao, Tang & He, 2014; Li *et al.* 2014, 2017*a*,*b*; Liu *et al.* 2017*b*).

The Alxa block in westernmost Inner Mongolia of China is located at the triangle connecting the North China Craton to the east, the Tarim Craton to the west and the southernmost CAOB to the north (Fig. 1a, b). A Permian subduction system has been proposed to account for the lithostratigraphic and magmatic rocks in the northern Alxa block (Wu, He & Zhang, 1998; Feng *et al.* 2013; Zheng *et al.* 2014; Liu *et al.* 2017*b*), and the Enger Us fault zone represents a part of the Tianshan–Solonker suture zones (Xiao *et al.* 2003; Feng *et al.* 2013; Zheng *et al.* 2014). However, the study of the Late Palaeozoic magmatic rocks in the

†Author for correspondence: wanghua@cug.edu.cn

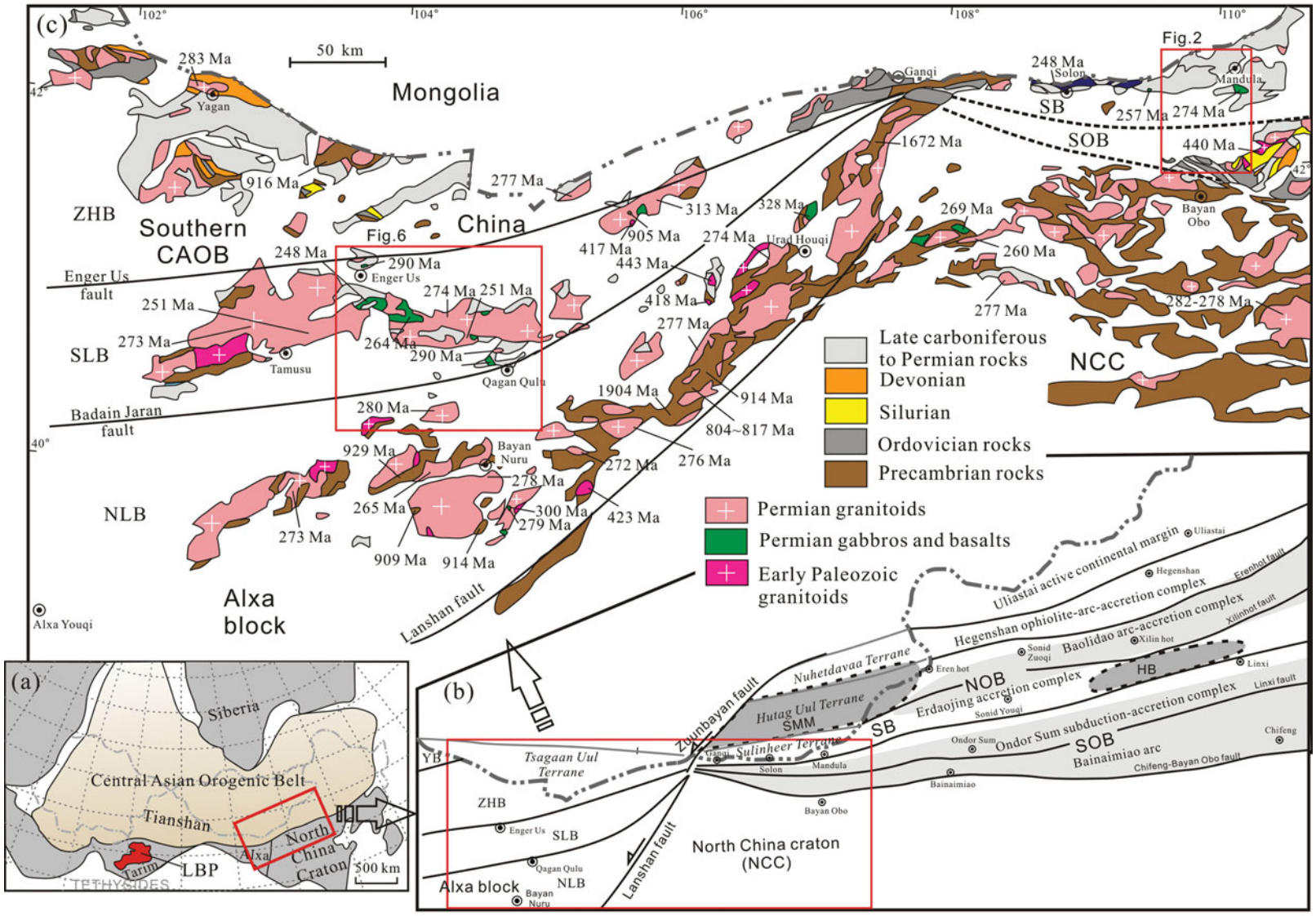

Figure 1. (Colour online) (a) Simplified tectonic sketch map of China showing the location of the Alxa block and relationships with the North China Craton (NCC) and the Central Asian Orogenic Belt (CAOB). (b) Tectonic division of the CAOB in eastern Inner Mongolia and the Alxa region (after Badarch, Cunningham & Windley, 2002; Xiao *et al.* 2003; Jian *et al.* 2008; Xu *et al.* 2013; Zheng *et al.* 2014; Liu *et al.* 2017*a*). (c) Geological map of the Alxa block showing the distributions of the strata and magmatic rocks (modified after 1:200 000 geological maps from NMBGMR, 1991 and Shi *et al*. 2014). SLB – Shalazhashan Belt; NLB – Nuru–Langshan Belt; ZHB – Zhusileng–Hangwula Belt; LBP – large basalt province in the Tarim; NOB – Northern Orogenic Belt; SOB – Southern Orogenic Belt; NCC – North China Craton; HB – Hunshandake Block; SMM – Southern Mongolia Microcontinent.

Alxa block suggested an extensional setting triggered by the Tarim mantle plume (Dan *et al.* 2014*a*, 2015). The Late Palaeozoic tectonic settings in eastern Inner Mongolia are also hotly debated. For example, the Solonker Belt was considered as an Early Palaeozoic suture zone which was reworked by Permian extensional tectonics (Chen *et al.* 2012; Xu *et al.* 2013, 2014; Shao, Tang & He, 2014; Luo *et al.* 2016; Wang *et al.* 2016). By contrast, more studies tend to regard the Solonker Belt as a Late Palaeozoic zone, with Early Palaeozoic subduction zones distributing to its north and south (Xiao *et al.* 2003, 2015; Li *et al.* 2014, 2017*a*,*b*; Eizenhöfer *et al.* 2015*a* ,*b*; Liu *et al.* 2017*a*).

The provenance of the clastic rocks can help us better understand the tectonic history of the southernmost CAOB, and studies have been intensively carried out in eastern Inner Mongolia (e.g. Li *et al.* 2011; Eizenhöfer *et al.* 2014; Chen, Zheng & Zhao, 2016) and the Tianshan orogens in NW China (e.g. Choulet *et al.* 2012*a* ,*b*; Rojas-Agramonte *et al.* 2014; Zhang *et al.* 2014*b*). However, provenance analysis in western Inner Mongolia is rare, which hinders our understanding of the CAOB in this region. The Upper Carboniferous to Permian sandstones in the northern Alxa block contain information about the depositional environment, source characteristics, palaeogeography and tectonic setting (Han *et al.* 2012; Zhang *et al.* 2013*b*; Shi *et al.* 2016). This study collected six samples in western Inner Mongolia, including four sandstone samples in the Shalazhashan Belt (to the north of the Alxa block) and two samples in the Solonker Belt (in the Mandula area) to analyse their framework petrography, zircon morphology, U–Pb geochronology and Hf isotopes. Combining the new data with the previous studies, we can better unravel the tectonic-palaeogeographic history of the CAOB in western Inner Mongolia.

2. Geological setting

2.a. Lithotectonic units

2.a.1. The northern Alxa block

The northern Alxa block includes four tectonic belts from north to south, namely, the Yagan Belt, the Zhusileng–Hangwula Belt, the Shalazhashan Belt and the Nuru–Langshan Belt (Fig. 1b) (Wu, He & Zhang, 1998; Zheng *et al.* 2014; Liu *et al.* 2017*a*). The Yagan and Zhusileng–Hangwula belts crop out predominantly in the form of Carboniferous and Permian volcanic and volcaniclastic rocks, which unconformably cover the Silurian to Devonian sedimentary rocks and the Precambrian basement rocks composed of granitic gneiss, schist, migmatite, marble, quartzite and metasandstone of Mesoproterozoic to Neoproterozoic ages (e.g. NMBGMR, 1991; Wang, Wang & Wang, 1994; Wu, He & Zhang, 1998; Wang *et al.* 2001). Wang *et al.* (2001) and Zhou *et al.* (2013), respectively, reported zircon U–Pb ages of 916 ± 16 Ma and 905 ± 6 Ma for the granitic gneiss in the Zhusileng–Hangwula Belt (Fig. 1).

The Shalazhashan Belt is separated by the Enger Us fault from the Zhusileng–Hangwula Belt and contains minor Early Palaeozoic magmatic rocks (Fig. 1b), but widespread Late Palaeozoic magmatic plutons including voluminous 247–301 Ma granitoids and minor 249–264 Ma diorites and gabbros (e.g. Dan *et al.* 2014*a*; Liu *et al.* 2017*a*). The Shalazhashan Belt crops out as sedimentary rocks of the Upper Carboniferous to Permian Amushan Formation, which is composed of volcanic and volcaniclastic rocks, and neritic carbonates and clastic rocks (e.g. Bu *et al.* 2012; Zhang *et al.* 2013*b*; Shi *et al.* 2016).

The Nuru–Langshan Belt, separated by the Badain Jaran fault from the Shalazhashan Belt, is predominantly composed of Precambrian basement rocks including high-grade metamorphic supracrustal rocks with a deposition age of ∼ 2.7 Ga and metamorphic ages ranging from 2.5 to 2.7 Ga and 1.9 to 2.0 Ga (Geng *et al.* 2007), and Palaeoproterozoic gneisses, meta-clastic rocks and meta-carbonatites (NMBGMR, 1991; Li, 2006; Hu *et al.* 2014). The Neoproterozoic strata, designated the Langshan group, are composed of meta-sandstones and volcanic intercalations with ages of 0.7–1.0 Ga. The meta-sandstones have detrital zircon age groups of 1.35 Ga, 1.5–1.6 Ga, 1.7–1.8 Ga and 2.4–2.6 Ga (Hu *et al.* 2014). The Neoproterozoic granites are *c*. 0.8–1.0 Ga, and the Early Palaeozoic diorites and granitoids are *c*. 420–460 Ma. Late Palaeozoic mafic to felsic magmatic rocks with ages of *c*. 260–310 Ma are distributed in the Nuru–Langshan Belt (Geng & Zhou, 2010; Dan *et al.* 2012, 2014*b*, 2015; Wu *et al.* 2014; Liu *et al.* 2017*a*; Wang *et al.* 2016).

The Langshan fault that separates the Alxa block from the North China Craton is a NE-trending sinistral shear fault. It occurred at *c*. 250 Ma (Zhang *et al.* 2013*a*; Fig. 1b, c).

2.a.2. The northern margin of the North China Craton (the Bayan Obo–Mandula areas)

Three main lithotectonic units are recognized from the Bayan Obo area ranging up to the Mandula area, namely, the North China Craton, the Southern Orogenic Belt and the Solonker Belt (Fig. 1b, c).

The North China Craton in the Bayan Obo area crops out as basement rocks of Neoarchaean–Palaeoproterozoic granitic gneisses and paragneisses with zircon U–Pb ages of ∼ 2.5 Ga and 1.8–2.0 Ga (Fan *et al.* 2010; Liu *et al.* 2011, 2017*c*). The Meso- to Neoproterozoic Bayan Obo Group unconformably overlies these basement rocks and is composed of a thick sequence of low-grade metamorphosed supracrustal rocks, with detrital zircon U–Pb ages of 2.48–2.52 Ga, 1.85–1.95 Ga, 1.61–1.74 Ga, 1.53–1.55 Ga, 1.34–1.37 Ga and 1.13–1.18 Ga Liu *et al.* (2017*c*). These rocks are unconformably overlain by Carboniferous–Permian strata (NMBGMR, 1991). Also, 1.31–1.35 Ga mafic sills, A-type granites and carbonatite dykes are found in the North China Craton

https://doi.org/10.1017/S0016756817000978 Published online by Cambridge University Press

(Zhang *et al.* 2009*c* , 2012; Shi *et al.* 2012*a*; Fan *et al.* 2014). Late Palaeozoic granitic plutons are widespread along the northern margin of the North China Craton (Zhang *et al.* 2009*a* ,*b*, 2011; Chen *et al.* 2015; Pang *et al.* 2017).

The Southern Orogenic Belt, mainly exposed to the north of the E–W-striking Bayan Obo–Chifeng fault, consists of Ordovician to Early Silurian (*c.* 480 − 420 Ma) arc-related magmatic rocks and subduction accretionary complexes, and Upper Devonian sandstones (Jian *et al.* 2008; Shi *et al.* 2013; Xu *et al.* 2013). The Southern Orogenic Belt was created by the southward subduction of the Palaeo-Asian oceanic crust during Early Palaeozoic time (Tang, 1990; Jian *et al.* 2008; Xu *et al.* 2013) or southward episodic subduction during Palaeozoic time (e.g. Zhang *et al.* 2009*a*; Chu *et al.* 2013; Peng *et al.* 2013; Li *et al.* 2014). Upper Carboniferous sedimentary rocks unconformably cover the pre-Devonian rocks and in turn are intruded by Permian igneous plutons (NMBGMR, 1991).

The Solonker Belt comprises a series of Upper Palaeozoic turbidites and small amounts of limestones, which were deposited in shallow- to deep-water environments (Shao, 1991; Shang, 2004). Ultramafic/mafic rocks generally crop out as lenses within the turbidites or mafic sills intruding into the sedimentary rocks (e.g. Shao, 1991; Xiao *et al.* 2003). The mafic rocks commonly show arc- or MORB-like geochemical features (e.g. Jian *et al.* 2010; Luo *et al.* 2016). Voluminous Permian acidic volcanic rocks and equivalent intrusions are also widespread in the Solonker Belt (NMBGMR, 1991; Zhang *et al.* 2017).

3. Geology of the study areas

3.a. The Mandula area (the Solonker Belt)

3.a.1. Upper Palaeozoic sedimentary rocks

The Mandula area mainly exposes the Upper Carboniferous to Permian sedimentary and magmatic rocks (Figs 2, 3). The southern part of the Mandula area is dominated by limestones and sandstones ascribed to the Upper Carboniferous to Lower Permian Amushan Formation (C_2–P_1a, NMBGMR, 1991; the sandstone-rich units in the Amushan Formation are separated as the Benbatu Formation by BGIM, 2004 and Chen, Zheng & Zhao, 2016). However, these limestones are olistoliths cemented into a siltstone-greywacke matrix and thus the rocks are considered as an olistostrome (G. Shi, unpub. Ph.D. thesis, Univ. d'Orléans, 2013). The olistostrome is characterized by metre- to kilometre-sized blocks of limestone, sandstone and volcanic rock. Based on the lithology of the block, the olistostrome can be divided into two types: sandstone-rich and limestone-rich. The sandstone-rich olistostrome is characterized by angular clasts and blocks of coarse sandstone, decimetres to several tens of metres in size, and subordinate and smaller, rounded clasts, and the matrix is greyish greywacke (Fig. 4a). The limestone-rich olistostrome contains limestone blocks ranging from kilometre- to metre-scale in the exposed longest dimension, and the matrix is greyish-green to dark grey and consists of slightly sandy mudstone (Fig. 4b). Rounded limestone blocks are occasionally found in the well-stratified turbidite of the Baotege Formation. The limestone olistoliths contain fossils of the *Sphaeroschwagerina* Biozone that is originally found in the limestones of the Amushan Formation exposed in the Southern Orogenic Belt. The olistostrome occurs mostly in the upper part of the Amushan Formation, particularly in the southern part of the Mandula area. The sandstone-rich olistostrome, ∼ 1 km in width, occurs in the southern portion of the olistostrome, and the limestone-rich olistostrome, about 2–5 km in width, occurs in the northern portion of the olistostrome, transiting into the turbidite of the Baotege Formation.

The Lower Permian Baotege Formation (P_1b) and a basaltic lava unit dated as 274 Ma (Chen *et al.* 2012) crop out to the north of the olistostrome. The Baotege Formation is composed of well-stratified turbidites and intercalations of volcanic rocks (Fig. 3). The turbidite lithological types include thick- to medium-bedded sandstone, thick-bedded sandstone–mudstone couplets, thin-bedded sandstone–mudstone couplets, siltstone–mudstone laminae and chert.

The thick- to medium-bedded sandstone commonly forms packets ranging from 0.5–10 m thick. The sandstone is light brown, fine- to medium-grained, and massive to poorly horizontally laminated. Beds are commonly amalgamated and contain rare mudstone rip-up clasts at the basal level. The thick- to medium-bedded sandstone occurs mostly to the north of the olistostrome. Packets of thick- to medium-bedded sandstone are laterally continuous extending to the sandstone–mudstone couplets.

The thick-bedded sandstone–mudstone couplets form packets ranging from 0.1–50 m thick. The sandstone parts of the couplets are grey and fine grained, with Bouma (1962) Tcd divisions common and Tabcd divisions rare (Fig. 4c). Rip-up clasts of black mudstone are commonly present at the base of the couplets. The mudstone parts of the couplets are black and display Bouma (1962) Te divisions, or commonly grade into lime mudstone.

The thin-bedded sandstone–mudstone couplets are the most dominant lithological type and form packets up to 300 m thick in the outcrops. The sandstone parts of the couplets are light brown to dark grey and fine grained, with Bouma (1962) Tcd divisions common. Locally, the sandstone is tuffaceous. The mudstone parts of the couplets are black and display Bouma (1962) Tde divisions, or commonly grade into lime mudstone.

The siltstone–mudstone laminae lithological type is characterized by thin regular siltstone–mudstone laminae (Fig. 4d), forming packets ranging from 0.5–20 m thick. The siltstone parts of the laminae are light grey and the mudstone parts of the laminae are black

https://doi.org/10.1017/S0016756817000978 Published online by Cambridge University Press

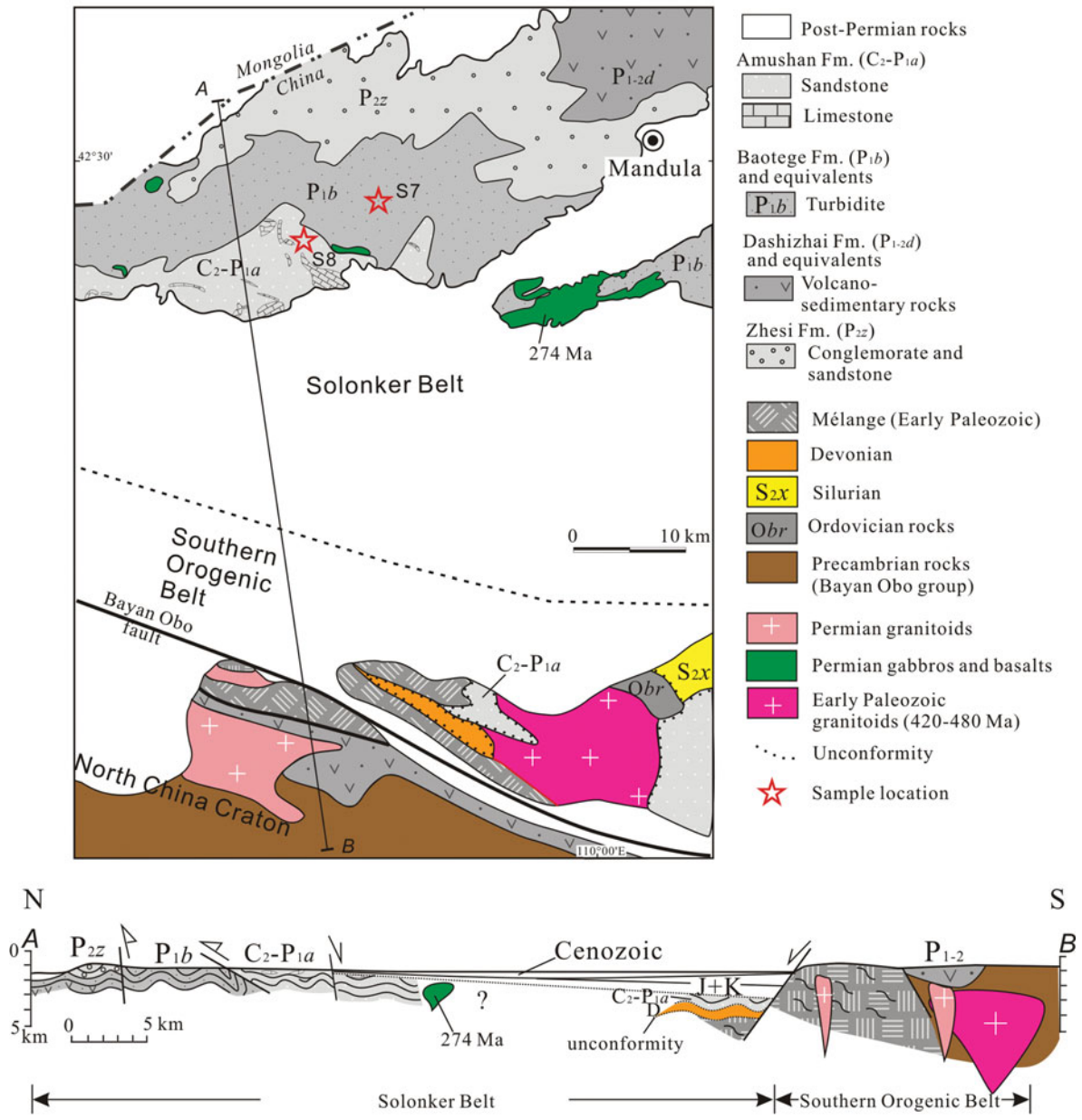

Figure 2. (Colour online) Geological map of the Mandula area demonstrating the lithostratigraphic and magmatic rocks and tectonic division. The age of the basalt is according to Chen *et al*. (2012).

and display Bouma (1962) Te divisions, or commonly grade into lime mudstone or chert.

The chert is massive or slightly laminated, 3–5 m in thickness (Fig. 4e). The chert commonly occurs in the northwest of the Mandula area and contains radiolarian faunas (Wang *et al*. 2005).

The Middle Permian Zhesi Formation (P_2z) is *c*. 700–1000 m thick and comprises a lower part of mainly turbidite intercalated with limestone lenses, and an upper part of reddish and grey thick massive limestone and reef, conglomerate, coarse-grained sandstone and calcareous sandstone (Fig. 3). The turbidite of the Zhesi Formation is dominated by the lithological types of thick-bedded sandstone–mudstone couplets and thin-bedded sandstone–mudstone couplets, which are similar to the rhythm types of the Baotege Formation. The mudstone parts of couplets are black and commonly grade into lime mudstone or limestone lenses.

The upper part is dominated by massive limestone overlying the lower turbidite, a fringing reef extending several kilometres and an isolated reef body above sandstones, with a mixed fauna of Boreal, Tethyan and endemic elements (NMBGMR, 1991; Wang *et al.* 2005; Shen *et al.* 2006).

The conglomerate is characterized by disorganized pebbly sandstone, forming beds of 0.1 to 1 m thick (Fig. 4f). It is dark grey and consists of *c*. 40 % clasts and 60 % matrix. The clasts are well-rounded sandstone, mudstone, volcanic rocks and limestone in order of decreasing abundance. Occasionally, outsized limestone clasts (up to 2 m) are present in the conglomerate. The conglomerate commonly shows massive, weakly stratified or normally graded structures and

https://doi.org/10.1017/S0016756817000978 Published online by Cambridge University Press

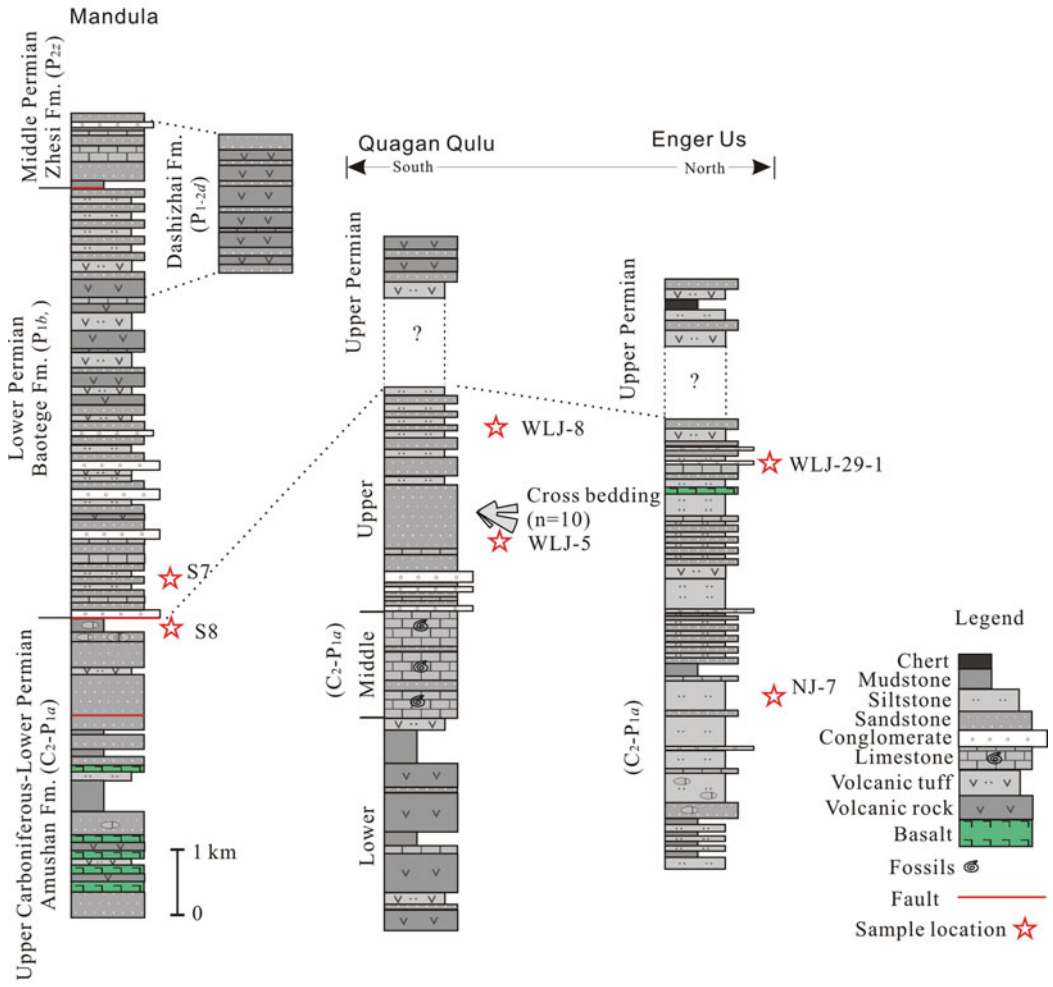

Figure 3. (Colour online) Stratigraphic columns of the Mandula, the Quagan Qulu and the Enger Us areas (modified after NMBGMR, 1991; Shi *et al.* 2016).

mainly forms thick lens-shaped beds, laterally discontinuous in outcrops.

In the north of the Mandula area, the Lower–Middle Permian Dashizhai Formation ($P_{1\text{-}2}d$) has the lithological composition of basaltic andesite, rhyolite, tuff, sandstone and silty mudstone (Zhang *et al.* 2008; Shao, Tang & He, 2014; Zhang *et al.* 2017).

3.a.2. Other rocks in the Mandula area

The Southern Orogenic Belt exposed in the south of the Mandula area includes the subduction-related mélange rocks and the arc magmatic rocks with ages of *c*. 480–420 Ma (Fig. 2). These rocks are unconformably overlain by the Upper Silurian to Lower Devonian sedimentary successions of limestones and sandstones (Shi *et al.* 2013; Chen, Zheng & Zhao 2016; Zhang & Zhang, 2016). The Upper Carboniferous to Lower Permian Amushan Formation, unconformably overlying the Lower Palaeozoic rocks, is mainly composed of limestones, sandstones, silty mudstones and volcanic rocks, with a fossil assemblage of brachiopods, corals, ammonoids and fusulinids of the *Sphaeroschwagerina* Biozone and *Triticites* Biozone, suggesting a shallow-marine sedimentary environment (Yang *et al.* 2015).

The rocks exposed in the North China Craton include the Meso- to Neoproterozoic Bayan Obo Group and the Permian volcanic rocks and granitic plutons (NMBGMR, 1991; Chen *et al.* 2015). The Bayan Obo Group consists of conglomerate, sandstone and limestone deposited in a rifted basin Liu *et al.* (2017*c*).

3.b. The Shalazhashan Belt

3.b.1. Upper Palaeozoic sedimentary rocks

The Upper Palaeozoic strata in the Shalazhashan Belt crop out well in the Quagan Qulu area and the Enger Us area, and include the Upper Carboniferous to Lower Permian Amushan Formation and undifferentiated Upper Permian volcano-sedimentary rocks (Figs 3, 5). The Amushan Formation in the Quagan Qulu area includes three members (NMBGMR, 1991).

The lower member is predominantly composed of basaltic to dacitic volcanic rocks, volcaniclastic rocks, silty slate and minor limestone lenses, with fossils of the *Triticites* Biozone. The middle member, with a total

https://doi.org/10.1017/S0016756817000978 Published online by Cambridge University Press

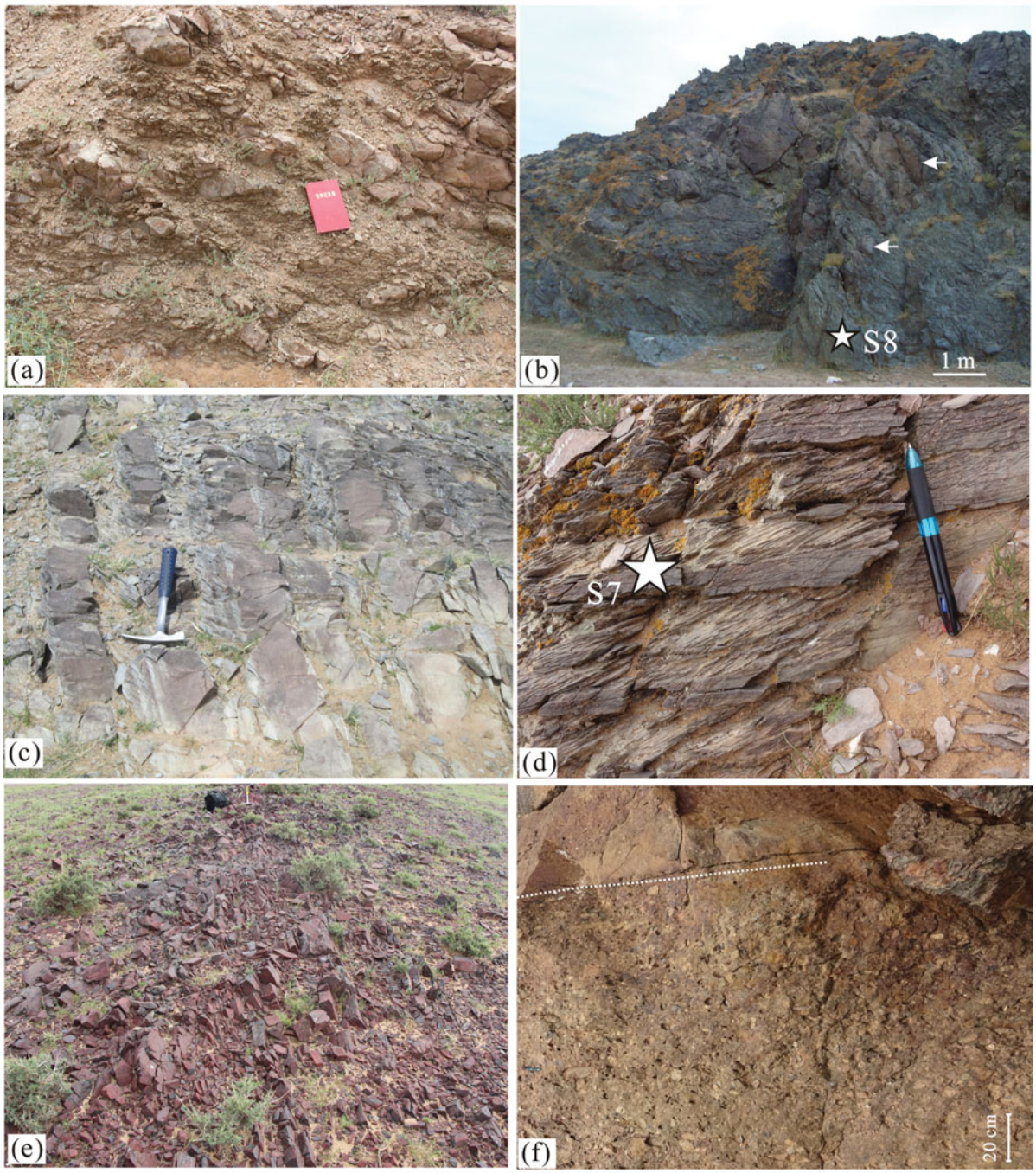

Figure 4. (Colour online) Field photographs of the Upper Palaeozoic sandstones in the Mandula area. (a) The sandstone-rich olistostrome is dominated by various-sized blocks of sandstone. (b) The limestone-rich olistostrome is dominated by large-sized blocks of limestone and smaller sandstone; it represents a mixture of intrabasin autochthonous sediments and allochthonous limestones from the Early Palaeozoic orogens (the Southern Orogenic Belt). The white arrows mark the olistoliths of limestones. Sample S8 was taken from the matrix of the olistostrome. (c) The thick-bedded sandstone–mudstone couplets have common Bouma (1962) Tcd divisions and rare Tabcd divisions. (d) The siltstone–mudstone laminae are composed of light grey siltstone and black mudstone. Sample S7 is taken from the fine-grained sandstone. (e) The red chert occurs as lenses in the turbidites in the Mandula area. (f) The conglomerate in the Zhesi Formation, *c*. 1 m thick, is composed of parallel pebbles. The hammer for scale is 30 cm long, the notebook is 20 cm long and the pen is 13 cm long.

thickness of 700–2000 m, is composed of thick- to medium-bedded limestone, calcareous sandstone and thin-bedded oolitic limestone and conglomeratic limestone. The limestones contain fossils of corals, brachiopods, ammonoids and fusulinids (Bu *et al.* 2012).

The upper member of the Amushan Formation consists of a lower sandstone-dominated sequence and upper fine-grained sequence, with a thickness of 2 km or more. The lower sandstone is composed of metre-scale beds of coarse sandstone, pebbly sandstone and thin-bedded conglomerate (Fig. 6a). Bedding in the sandstone is tabular and commonly has cross-stratification (Fig. 6b). The upper fine-grained sequence is composed of red mudstone, siltstone and centimetre- to

https://doi.org/10.1017/S0016756817000978 Published online by Cambridge University Press

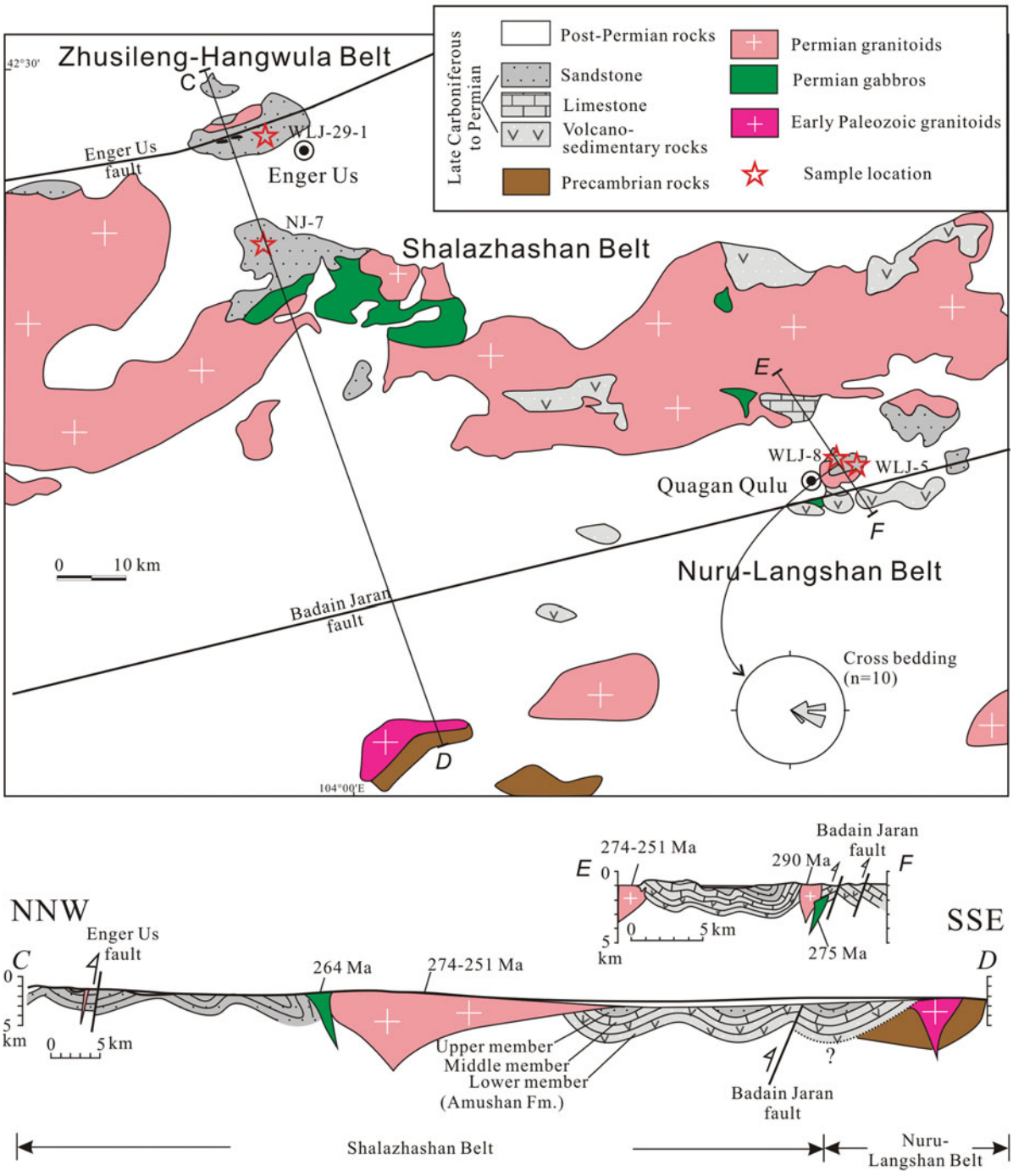

Figure 5. (Colour online) Geological map of the Quagan Qulu and Enger Us areas and tectonic divisions (modified after Zheng *et al.* 2014).

decimetre-scale interbeds of fine to coarse sandstone. The fine-grained lithologies are thick tabular beds of rippled or plane-laminated sandstone. Some beds, occurring within the mudstone, have sharp bases that grade upwards into massive or laminated siltstone, typical of Bouma sequence Tde divisions (Fig. 6c). The middle and upper members contain fusulinid fossils of the *Pseudoschwagerina* Biozone, indicative of Late Carboniferous to Early Permian ages (NMBGMR, 1991; Zhang *et al.* 2013*b*). The Upper Permian in the Quagan Qulu area is composed of sandstones and volcanic rock intercalations of 254 Ma (Shi *et al.* 2016).

The Enger Us area is characterized by a thick succession of thin-bedded fine-grained sandstone, siltstone, tuffaceous siltstone, shale and chert, with several beds of thin- to medium-bedded sandstone–mudstone couplets. In macroscopic view, basalts dated at 302–290 Ma are lenses cemented within the beds (Zheng *et al.* 2014; Shi *et al.* 2016). The chert is commonly red, thin bedded, massive or laminated and can be laterally continuous for several decametres (Fig. 6d). The thin-bedded, fine-grained sandstone and siltstone are brown, dark grey and often form rhythmic laminae (Fig. 6e). The sandstone–mudstone couplets

https://doi.org/10.1017/S0016756817000978 Published online by Cambridge University Press

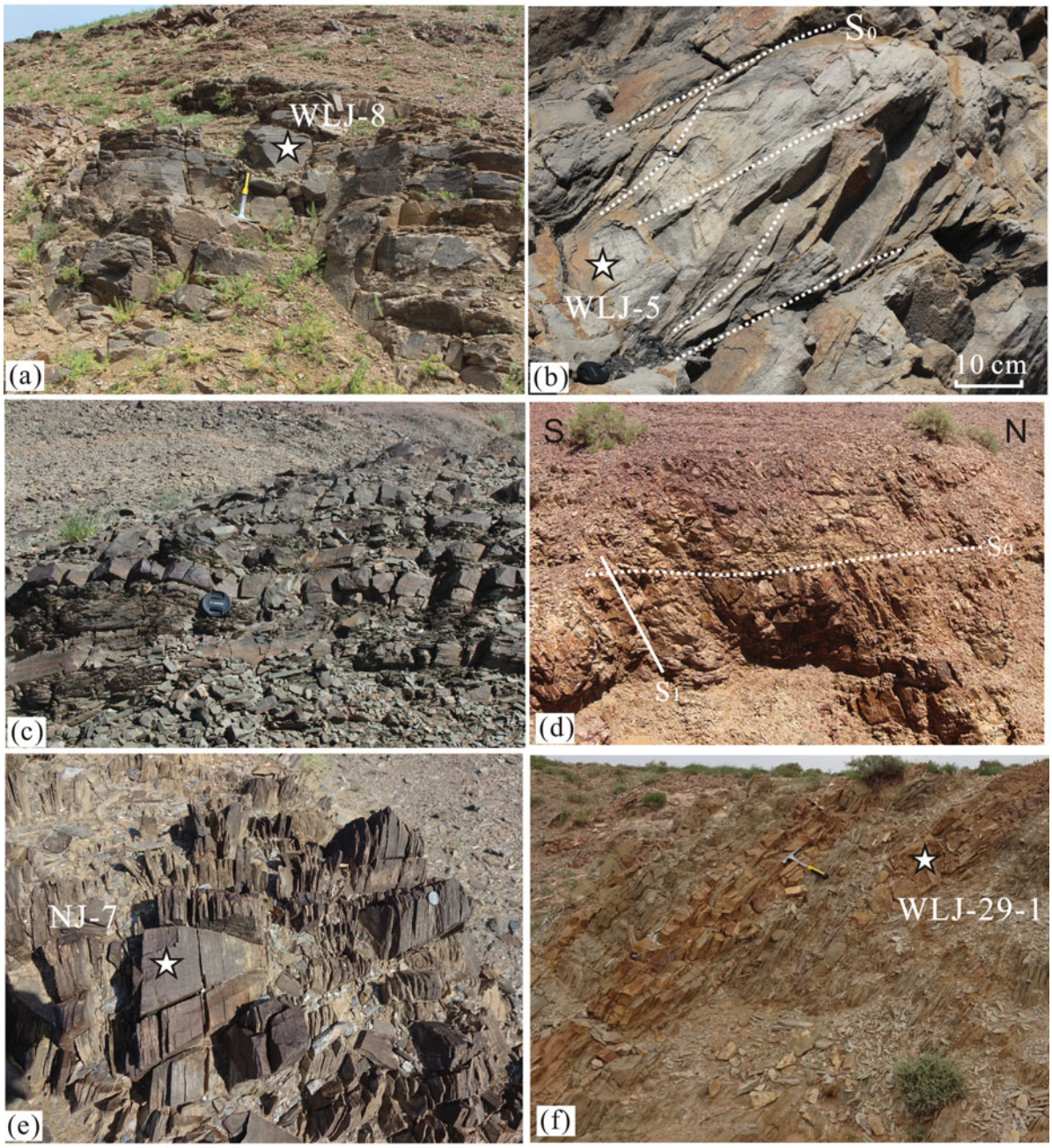

Figure 6. (Colour online) Field photographs of the Upper Member of the Amushan Formation in the Quagan Qulu area. (a) The thick-bedded coarse sandstone in the lower part of the Upper Member of the Amushan Formation, where the sample WLJ-8 was taken from. (b) Locally the thick-bedded coarse sandstone developed cross-stratification, where the sample WLJ-5 was taken from. (c) The thin-bedded sandstone and mudstone couplets in the upper part of the Upper Member of the Amushan Formation. (d) The intercalation of the red chert (upper) and the tuffaceous siltstone (middle). The rocks develop N-dipping foliation (S1). (e) The rhythmic laminae of fine-grained sandstone and siltstone in the Enger Us area, where the sample NJ-7 was taken from. (f) The lens-shaped sandstone–mudstone couplets within the fine-grained dominant succession, where the sample WLJ-29-1 was taken from. The hammer for scale is 30 cm long and the lens cap is 7 cm in diameter.

are brown and lens-shaped forms within the shale (Fig. 6f), and the sandstone bed normally has pebbly sandstone at the base and is upward-grading into siltstone or mudstone.

One outcrop in the Enger Us area, composed of a succession of siltstone, tuffaceous siltstone, mudstone and volcaniclastic rocks, has yielded a radiolarian fauna of late Middle Permian to early Late Permian age (Xie *et al.* 2014), confirming the deposition was occurring in Middle to Late Permian times. However, the detailed distribution and thickness of the Middle to Upper Permian deposits are not well known (Figs 3, 5).

3.c. Sampling

A total of six sandstone samples were collected for detrital zircon U–Pb dating, and three of them were further selected for Lu–Hf isotopic measurement.

https://doi.org/10.1017/S0016756817000978 Published online by Cambridge University Press

Table 1. Framework modes of the sandstone samples of the Upper Carboniferous to Permian sandstones in western Inner Mongolia

sample No.	lithology	Qm	Qp	Kf	Pl	F	Lv	Ls	Ms	Bi	M	Total	Qt	L	Lt
S7	fine-grained sandstone	35.3 %	4.2 %	9.5 %	11.3 %	20.8 %	27.6 %	5.6 %	2.3 %	0.0 %	4.2 %	100.0 %	39.5 %	35.5 %	39.7 %
S8	sandy mudstone	15.0 %	0.0 %	2.3 %	3.7 %	6.0 %	0.0 %	0.0 %	0.0 %	0.0 %	79.0 %	100.0 %	15.0 %	0.0 %	0.0 %
WLJ-5	coarse-grained sandstone	22.6 %	3.5 %	5.1 %	5.3 %	10.4 %	42.3 %	1.9 %	4.0 %	7.8 %	7.5 %	100.0 %	26.1 %	56.0 %	59.5 %
WLJ-8	coarse-grained sandstone	19.6 %	5.5 %	5.1 %	7.5 %	12.6 %	36.5 %	1.2 %	6.5 %	11.8 %	6.3 %	100.0 %	25.1 %	56.0 %	61.5 %
WLJ-29-1	coarse-grained sandstone	45.3 %	3.7 %	10.7 %	8.6 %	19.3 %	22.6 %	2.3 %	3.5 %	0.0 %	3.3 %	100.0 %	49.0 %	28.4 %	32.1 %
NJ-7	siltstone	42.5 %	2.2 %	6.8 %	7.2 %	14.0 %	17.6 %	5.2 %	5.3 %	0.0 %	13.2 %	100.0 %	44.7 %	28.1 %	30.3 %

Qm – monocrystalline quartz grains; Qp – polycrystalline quartz grains; Pl – plagioclase; Kf – K-feldspar; Lv – volcanic grains; Ls – sedimentary grains; Ms – muscovite; Bi – biotite; M – matrix. Qt = Qm + Qp where Qt is total quartz grains; F = Pl + Kf where F is total feldspar; L = Ls + Lv + Ms + Bi where L is lithic fragments. Lt = L + Qp where Lt is total lithic fragments.

Samples S7 and S8 were taken from the turbidites of the Baotege Formation (Lower Permian) and the matrix of the olistostromes, respectively (Figs 2, 4b, d). Samples WLJ-5 and WLJ-8 were taken from the coarse-grained sandstones in the Upper Member of the Amushan Formation in the Quagan Qulu area (Figs 5, 6a, b). Samples NJ-7 and WLJ-29-1 were taken from the turbidites in the Enger Us area (Figs 5, 6e, f).

4. Methodology

The petrographic texture and photomicrographs were studied using a polarized light microscope. The modal component statistics use the updated Gazzi–Dickinson counting method (Ingersoll *et al.* 1984; Dickinson, 1985).

Detrital zircons were separated from the very fine sand fraction (0.10–0.063 mm) using a heavy liquid with specific gravity of 2.84 g/cm^3. Then, zircon fragments were embedded in epoxy resin and polished to expose their inner structure. U–Pb dating, trace-element analysis and cathodoluminescence (CL) imaging were conducted by LA-ICP-MS at the Sample Solution Analytical Technology Co., Ltd, Wuhan. Detailed operating conditions and element correction follow Liu *et al*. (2008, 2010) and Lin *et al*. (2015). The dated grains were randomly selected without considering the grain shapes and internal structures, and the dating spots mainly focused on the core part of the zircon. Seventy grains were dated for each sample following the suggestion of Andersen (2005) that the random selection should comprise 35–70 grains or more depending on the complexity of the age distribution. The U–Pb ages of lower than 94 % concordance were not counted when calculating the relative probability for ^{206}Pb–^{238}U age using Isoplot/Ex_ver3 (Ludwig, 2003). The counted number of valid zircon ages is between 53 and 65, generally equivalent to the number of 59 suggested by Dodson *et al*. (1988).

After the dating, the grains with valid Palaeozoic ages were selected for *in situ* zircon Hf isotopic analysis. A total of 61 grains from samples S7, S8 and WLJ-29-1 were analysed. Zircon Hf isotopic analysis was conducted at the State Key Laboratory of Geological Processes and Mineral Resources, China University of Geosciences (Wuhan). Detailed operating processes were described by Hu *et al*. (2012). The crustal model age (T^C_{DM}) was calculated assuming that the parental magma was produced from an average continental crust (^{176}Lu/^{177}Hf = 0.015) that was originally derived from the depleted mantle. The ^{176}Hf/^{177}Hf and ^{176}Lu/^{177}Hf ratios of chondrite and depleted mantle at the present are 0.282772 and 0.0332, and 0.28325 and 0.0384, respectively (Blichert-Toft & Albarede, 1997; Griffin *et al.* 2004).

5. Results

5.a. Framework petrography

The detailed petrographic results are listed in Table 1.

Sample S7, sandstone taken from the turbidite (Baotege Formation) in the Mandula area, is fine grained, well sorted and composed of quartz (39.5 %), alkali feldspar (9.5 %, mostly orthoclase), plagioclase (11.3 %) and lithic fragments (35.5 %). The lithic fragments are predominantly volcanic rocks (27.6 %) and subordinately mudstone/siltstone fragments (5.6 %). The volcanic fragments are mostly composed of tiny acicular or scaly felsic minerals, and opaque materials (Fig. 7). A small amount of muscovite (2.3 %) is counted.

Sample S8, sandy mudstone taken from the matrix of the olistostrome in the Mandula area, is mostly composed of mudstone matrix (79.0 %), with grains of quartz and feldspar. The clastic grains are poorly sorted, ranging from ~ 0.1 mm to several centimetres (Fig. 7).

Sample WLJ-8, sandstone taken from the Upper Member of the Amushan Formation in the Quagan Qulu area, is coarse-grained sandstone, poorly sorted, angular to sub-angular in texture, showing characteristics of a low maturity of sandstone. The grain size varies considerably between 0.2 mm and 0.8 mm. It is composed of quartz (25.1 %), lithic fragments (56.0 %) and feldspar (12.6 %). Volcanic rock (36.5 %) predominates in the lithic fragments. There is a significant

https://doi.org/10.1017/S0016756817000978 Published online by Cambridge University Press

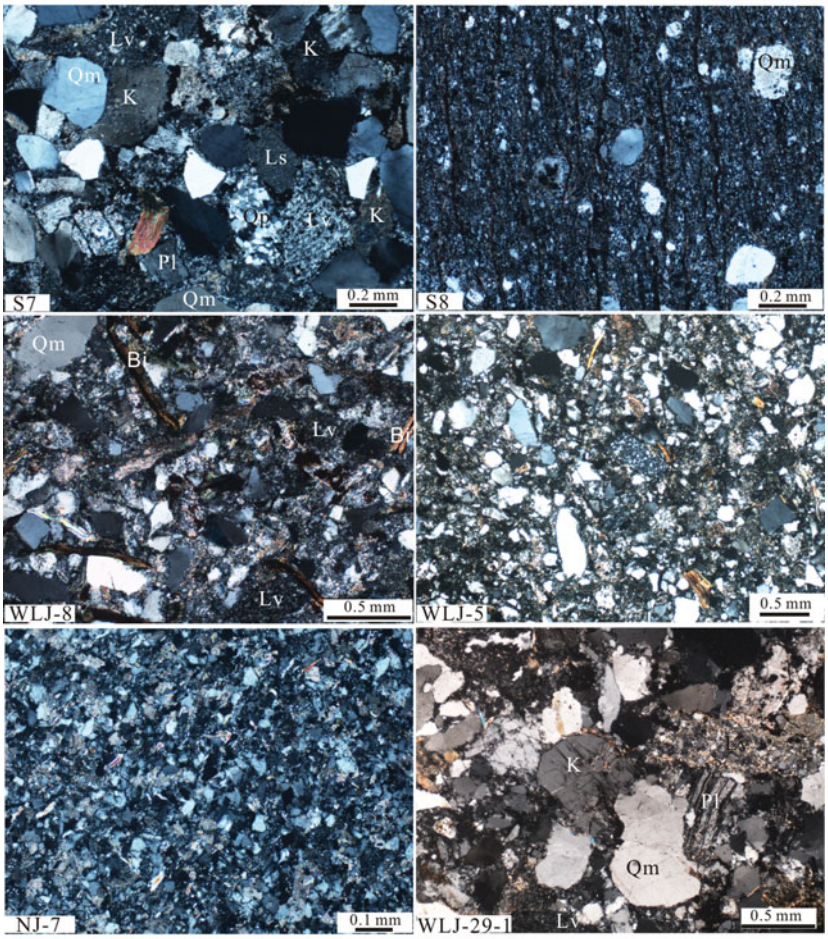

Figure 7. (Colour online) Petrographic photographs of the sandstones in the Solonker Belt (S7 and S8) and the Shalazhashan Belt (WLJ-5, WLJ-8, NJ-7, WLJ-29-1), in cross-polarized light. Lv – volcanic fragments; Bi – biotite; Ms – muscovite; Qm – monocrystalline quartz; Qp – polycrystalline quartz; Pl – plagioclase; K – K-feldspar.

amount of biotite (11.8 %) and muscovite (6.5 %). The biotite is commonly curved owing to grain compression (Fig. 7).

Sample WLJ-5, sandstone taken from the Upper Member of the Amushan Formation in the Quagan Qulu area, is texturally immature, with very low degrees of rounding and sorting, and with grain sizes ranging from 0.2 mm to 0.6 mm (Fig. 7). It comprises quartz (26.1 %), feldspar (10.4 %) and abundant lithic fragments (56.0 %). The proportion of the biotite and muscovite reaches up to 11.8 %. Lithic fragments are mainly of a volcanic type (42.3 %).

Sample NJ-7, siltstone taken from the turbidite in the Enger Us area, is quite fine grained (Fig. 7), well sorted and comprises quartz (44.7 %), lithic fragments (28.1 %) and feldspar (14.0 %). The proportions of volcanic, sedimentary fragments and muscovite are 17.6 %, 5.2 % and 5.3 %, respectively.

Sample WLJ-29-1, sandstone taken from the turbidite in the Enger Us area, is coarse grained, poorly sorted, sub-angular to sub-rounded in texture, and a few framework grains have developed cracks. It contains quartz (49.0 %), lithic fragments (28.4 %) and feldspar (19.3 %). It has a significant amount of volcanic fragments (22.6 %). Mudstone matrix is rare. The feldspar consists of alkali feldspar (mostly perthite) and plagioclase (Fig. 7).

5.b. Zircon U–Pb geochronology

The zircon U–Pb isotopic dating results for the six samples are listed in online Supplementary Material Table S1 available at http://journals.cambridge.org/geo. The concordia and probability density plots are shown in Figures 8 and 9.

In the sample S7, 53 out of 70 grains are concordant. The zircons are predominantly Palaeozoic (255–550 Ma) and yield two main age groups: (a) 270–330 Ma with a significant peak at 290 Ma and a secondary peak at 320 Ma; and (b) 420–550 Ma with a peak at 460 Ma and a secondary peak at 420 Ma. The subordinate groups include 1.4–1.5 Ga, 1.8–1.9 Ga and 2.3–2.6 Ga.

In the sample S8, 64 grains are concordant. The zircons have two main age groups: (a) 270–330 Ma with a significant peak at 295 Ma and a secondary peak at 330 Ma; and (b) 420–500 Ma with a peak at 438 Ma. The subordinate groups include *c*. 1.8–2.0 Ga and 2.4–2.6 Ga. One grain was dated at *c*. 1.4 Ga.

https://doi.org/10.1017/S0016756817000978 Published online by Cambridge University Press

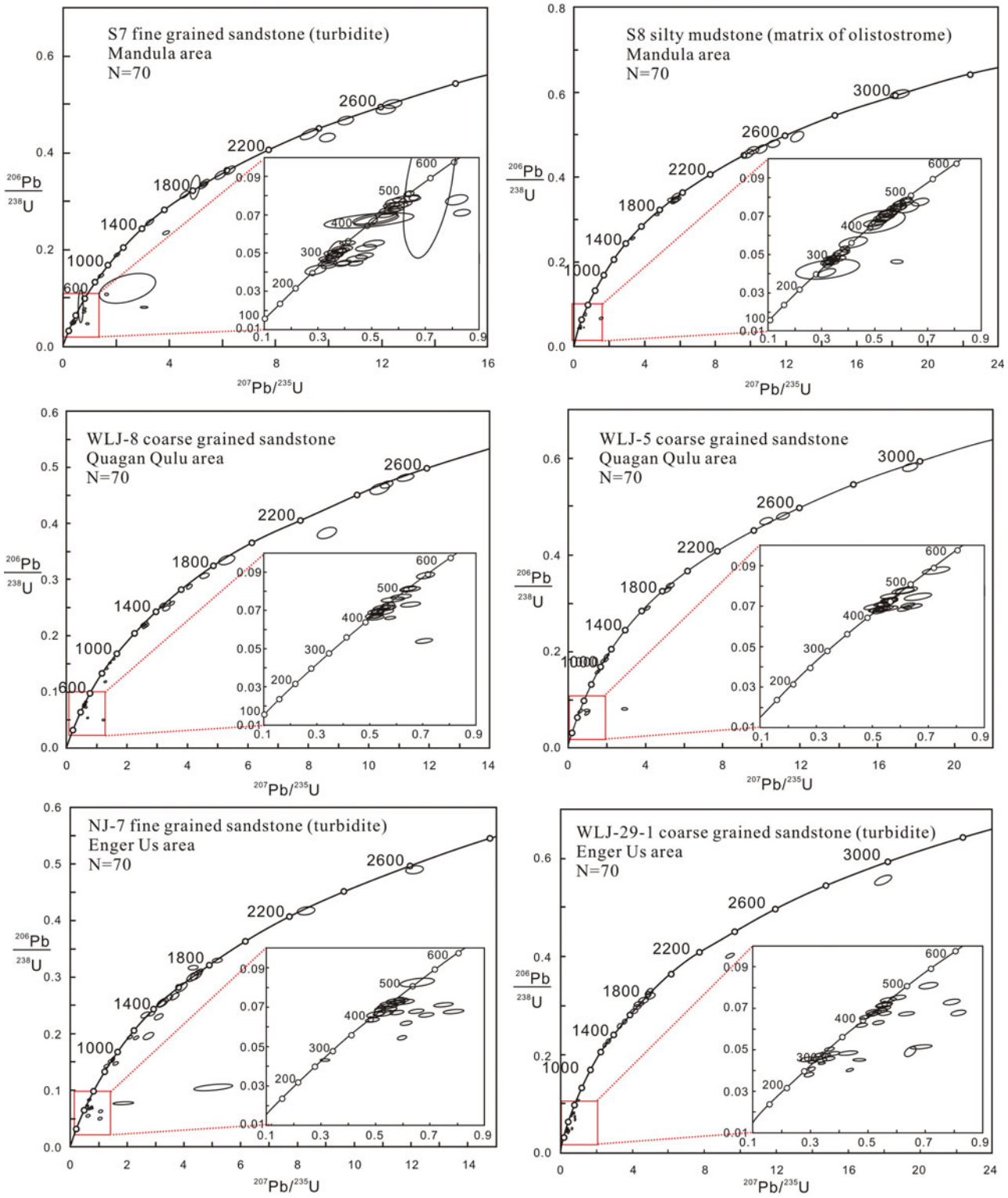

Figure 8. (Colour online) The representative chondrite-normalized rare earth element (REE) patterns of zircons from the studied samples. Chondrite normalization values from Sun & McDonough (1989). The related CL images of the marked zircons are in the online Supplementary Figures S1–S3 available at http://journals.cambridge.org/geo.

In the sample WLJ-5, 61 grains are concordant. The zircons have one main age group of 410–500 Ma with a significant peak at 433 Ma. The subordinate group is 0.9–1.0 Ga. Several zircon grains yield ages of *c*. 0.7 Ga, *c*. 1.9 Ga and *c*. 2.5 Ga.

In the sample WLJ-8, 64 grains are concordant. The zircons have one main age group of 410–550 Ma with a significant peak at 440 Ma. The subordinate groups include 0.9–1.0 Ga and 1.4–1.5 Ga. Several zircon grains yield ages of *c*. 1.2 Ga, *c*. 1.6 Ga and *c*. 2.5 Ga.

In the sample NJ-7, 55 grains are concordant. The zircons have one main age group of 420–500 Ma with a significant peak at 437 Ma. The subordinate

https://doi.org/10.1017/S0016756817000978 Published online by Cambridge University Press

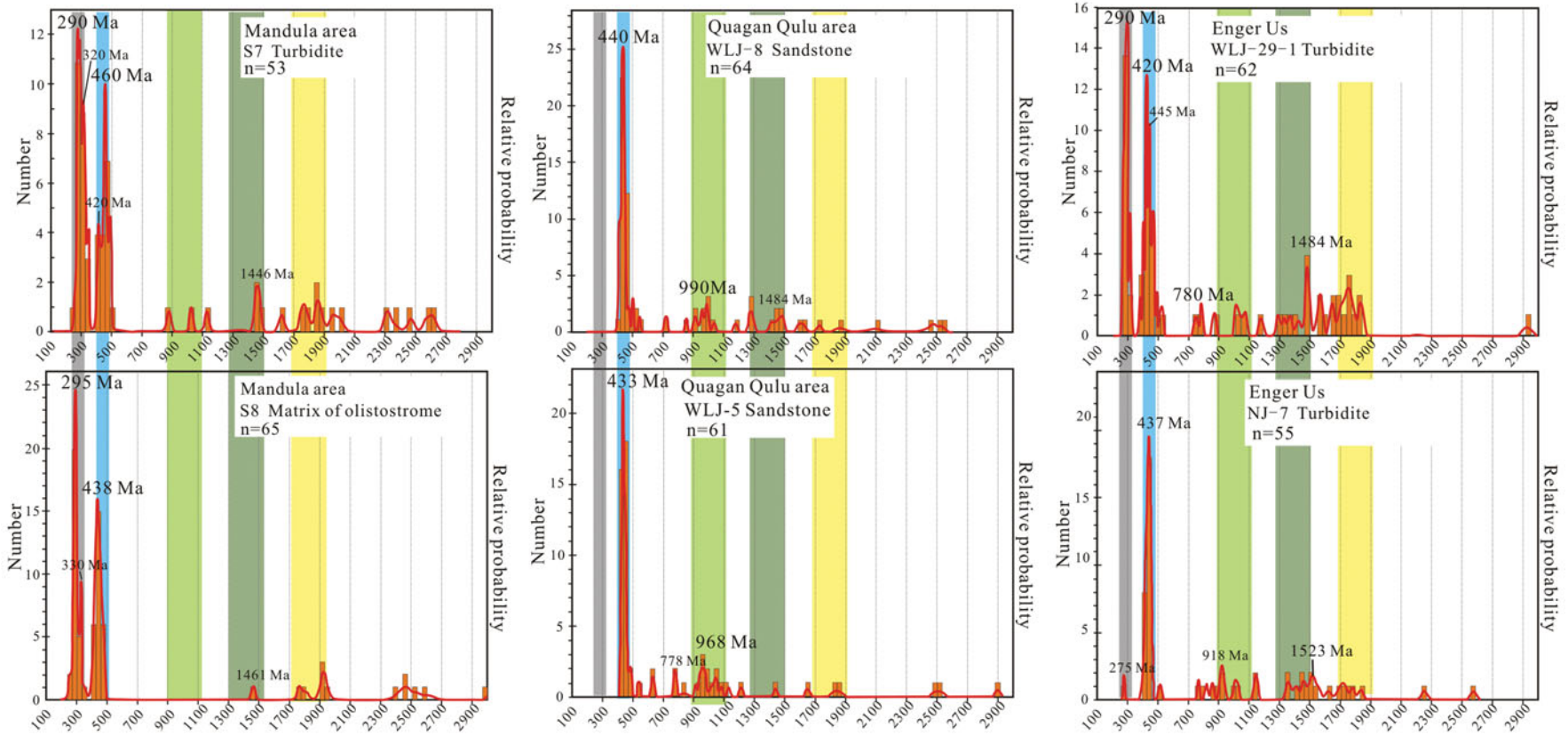

Figure 9. (Colour online) U–Pb concordia diagrams for zircons from the sedimentary rocks of the Solonker Belt (S7 and S8) and the Shalazhashan Belt (WLJ-8, WLJ-5, NJ-7, WLJ-29-1).

groups include 0.9–1.0 Ga and 1.4–1.6 Ga. Several zircon grains yield ages of ~ 275 Ma, ~ 800 Ma and 1.8–1.9 Ga.

In the sample WLJ-29-1, 62 grains are concordant. The zircons have two main age groups: (a) 270–310 Ma with a significant peak at 290 Ma, and (b) 400–550 Ma with a significant peak at 420 Ma. The subordinate groups include 1.3–1.5 Ga and 1.7–1.9 Ga. Several zircon grains yield ages of ~ 780 Ma and ~ 1000 Ma.

5.c. Zircon morphology

Most zircon crystals are euhedral in shape, with sizes ranging from 50 to 150 μm. We divided the zircons into six groups according to the U–Pb ages: (a) 2.3–2.6 Ga, (b) 1.7–2.0 Ga, (c) 1.2–1.7 Ga, (d) 0.7–1.2 Ga, (e) 400–550 Ma and (f) 260–330 Ma. All the measured zircons show various complicated internal textures (online Supplementary Material Figs S1, S2, S3 available at http://journals.cambridge.org/geo). The zircons of 2.3–2.7 Ga age are generally rounded in shape, with a dark, homogeneous texture, or dark rim with light inner core. Some zircons of 1.7–2.0 Ga age are subhedral and commonly have an inner core of clear oscillatory zoning but a dark, homogeneous rim, and some grains have misted textures with no clear zoning. The zircons of 1.2–1.7 Ga and 0.7–1.2 Ga ages are complicated in that some zircons have weak or clear oscillatory zoning, but some are homogeneous without zoning, or have a dark rim or patchy forms. The Palaeozoic zircon grains usually have a tetragonal and prismatic shape with oscillatory zoning. Most zircons of 400–550 Ma age have clear oscillatory zoning, but a few grains show irregular sectors without zoning. All the zircons of 260–330 Ma age have oscillatory zoning.

5.d. Zircon chemistry

The results of zircon chemistry for the six samples are listed in online Supplementary Material Table S2 available at http://journals.cambridge.org/geo. Most detrital zircons from our sedimentary samples have high Th/U ratios (> 0.10), and are enriched in heavy rare earth elements (HREEs) compared to light rare earth elements (LREEs), with positive Ce anomalies and marked negative Eu anomalies (Fig. 10). Some grains show relatively flat LREE patterns, no or weakly positive Ce anomalies (e.g. S7: a2, a3; WLJ-8: a1; WLJ-5: e6). Grain c6 of sample NJ-7 (1369 ± 32 Ma) has low LREE contents and Th/U ratio (< 0.10, see online Supplementary Material S2 available at http://journals.cambridge.org/geo). Grain b1 of sample S8 (1129 ± 32 Ma) exhibits a flat HREE pattern.

5.e. Lu–Hf isotopes

A total of 61 isotopic analyses were carried out on the dated detrital zircons of Palaeozoic ages (online Supplementary Material Table S3 available at http://journals.cambridge.org/geo). The Late Palaeozoic zircons from samples S7 and S8 have a dominant range from −5 to +7, with one grain having an extreme negative $\varepsilon_{Hf}(t)$ value of −17. The Early Palaeozoic zircons from sample S7 yield variable $\varepsilon_{Hf}(t)$ values from −7 to +8, with one grain ($\varepsilon_{Hf}(t) = -24$) plotting on the 3.0 Ga evolution line (Fig. 11). Most zircons from samples S7 and S8 plot in the East CAOB field (Yang *et al.* 2006).

The Late Palaeozoic zircons in sample WLJ-29-1 have $\varepsilon_{Hf}(t)$ values ranging from −5 to +11, and the Early Palaeozoic zircons yield $\varepsilon_{Hf}(t)$ values ranging from −9 to +5 (Fig. 11). The Late Palaeozoic zircons from WLJ-29-1 almost plot in the field of the Shalazhashan Belt, and the Early Palaeozoic zircons plot in the field of the Nuru–Langshan Belt. The zircons have a large range of T^{C}_{DM} ages (0.8–1.8 Ga), with a dominant population at 1.0–1.5 Ga (Fig. 11).

6. Discussion

6.a. Provenance analysis

6.a.1. The Solonker Belt (the Mandula area)

The limestone blocks in the olistostromes include fossils of the *Sphaeroschwagerina* Biozone, similar to the Amushan Formation exposed in the Southern Orogenic Belt, suggesting the Southern Orogenic Belt is one of the potential sources for the deposits of the Mandula area. This is consistent with the zircon age spectra that have an age peak at 438 Ma in sample S8 (the matrix of the olistostromes).

The zircons of 270–330 Ma age in samples S8 and S7 are subhedral to euhedral with variable zoning, high Th/U ratios (> 0.10), with positive Ce anomalies and marked negative Eu anomalies, which are diagnostic features of magmatic zircons (Hoskin & Ireland, 2000; Belousova *et al.* 2002; Corfu *et al.* 2003; Hoskin & Schaltegger, 2003). They might derive from two possible source areas, the northern margin of the North China Craton (including the Southern Orogenic Belt and the North China Craton) and the tectonic units of the CAOB (e.g. the Solonker Belt and the Northern Orogenic Belt; Jian *et al.* 2008; Xu *et al.* 2013). The Late Carboniferous to Permian magmatic rocks are widespread in the northern margin of the North China Craton, the Solonker Belt and the Northern Orogenic Belt (Chen *et al.* 2000; Zhang *et al.* 2008, 2009*a*, 2014*a*, 2017; Jian *et al.* 2010; Tong *et al.* 2010; Chen *et al.* 2012; Hu *et al.* 2015). However, the Late Palaeozoic magmatic rocks in the northern margin of the North China Craton (the Bayan Obo area) have more negative zircon ε_{Hf} values than that of the CAOB (Yang *et al.* 2006; Zhang *et al.* 2009*a*, 2011). Our zircon ε_{Hf} values mainly plot in the field of the CAOB and the overlapping field of the CAOB and the North China Craton, indicating that the Late Palaeozoic magmatic rocks in the tectonic units of the CAOB are the main

https://doi.org/10.1017/S0016756817000978 Published online by Cambridge University Press

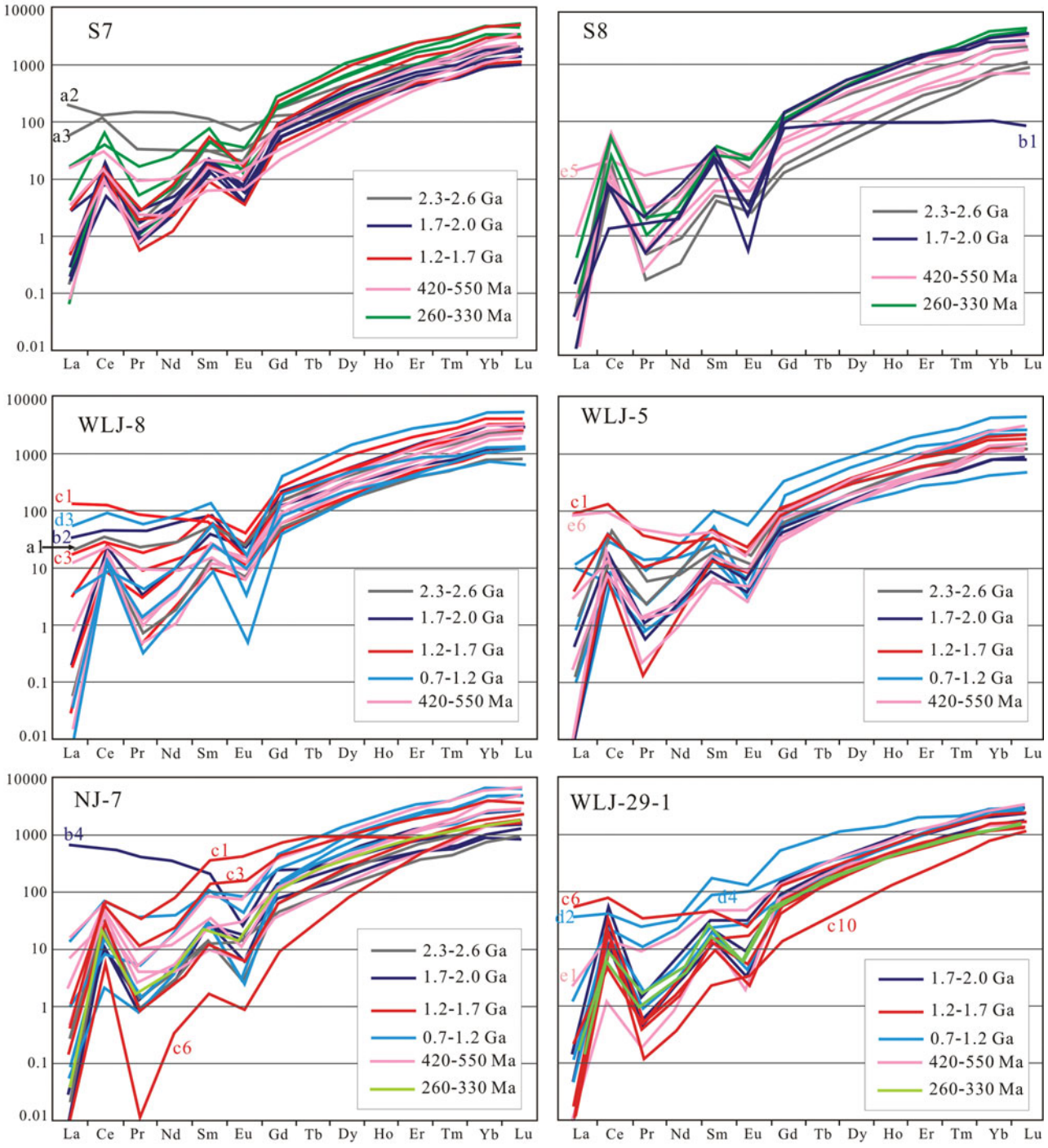

Figure 10. (Colour online) Relative probability plots and age histograms for the detrital zircons of the Solonker zone (the Mandula area) and the Shalazhashan Belt (the Quagan Qulu area and the Enger Us area) in western Inner Mongolia. The U–Pb ages with concordance errors smaller than 94 % are not counted (see online Supplementary Material Table S1 available at http://journals.cambridge.org/geo).

source. This is supported by the petrographic analysis, which shows the sandstones are immature, with a high proportion of volcanic fragments, suggesting a process of short distance transportation and proximal deposition. Moreover, the Late Palaeozoic zircons commonly have euhedral shapes, which is consistent with short distance transportation. Thus, we consider that the Late Palaeozoic volcanic rocks in the Solonker Belt and the Northern Orogenic Belt are the most plausible sources. The northern margin of the North China Craton as a subordinate source cannot be excluded owing to several zircons with negative zircon ε_{Hf} values.

The Early Palaeozoic zircons (420–550 Ma) have clear oscillatory zoning, positive Ce anomalies and marked negative Eu anomalies, which are common features of igneous zircons. These zircons are most probably derived from the Southern Orogenic Belt. Voluminous Early to Middle Palaeozoic ages of arc-related magmatic rocks have been documented in this

https://doi.org/10.1017/S0016756817000978 Published online by Cambridge University Press

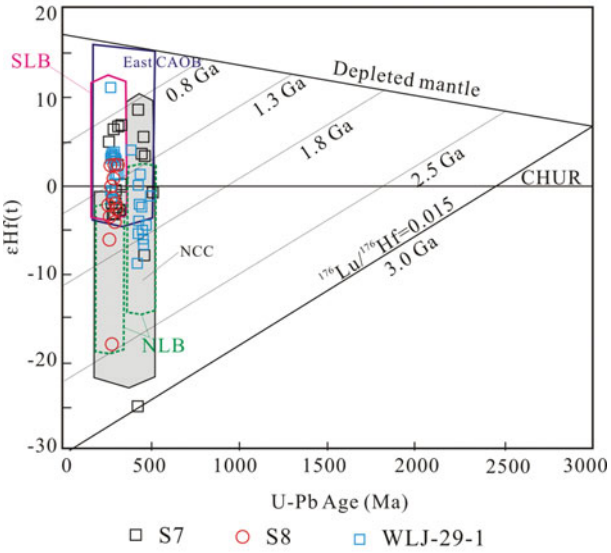

Figure 11. (Colour online) Plot of zircon U–Pb ages versus $\varepsilon_{Hf}(t)$ values. CHUR – chondritic uniform reservoir. The fields of the East CAOB and NCC are according to Yang *et al.* (2006) and Zhang *et al.* (2014*c*); and the fields of the Shalazhashan Belt and the Nuru–Langshan Belt are according to Dan *et al.* (2014*a*, 2015), Liu *et al.* (2017*b*) , Shi *et al.* (2014) and Zhang *et al.* (2015). CAOB – Central Asian Orogenic Belt; NCC – North China Craton; NLB – Nuru–Langshan Belt; SLB – Shalazhashan Belt.

belt in response to the southward subduction of the Palaeo-Asian Ocean (Jian *et al.* 2008; Xu *et al.* 2013; Zhang *et al.* 2014*c*; Fig. 12). The Lower to Middle Palaeozoic rocks of the Southern Orogenic Belt have a large range of zircon ε_{Hf} values (Zhang *et al.* 2014*c*). Our measured zircon ε_{Hf} values plot in a large range of –10 to +10 (Fig. 11). Considering the source of the limestone olistoliths, we suggest the Southern Orogenic Belt might provide clastic materials for the Carboniferous to Permian sandstones.

The Precambrian zircons might derive from the North China Craton. The Meso- to Neoproterozoic Bayan Obo Group contains detrital zircons of 2.48–2.52 Ga, 1.85–1.95 Ga, 1.61–1.74 Ga, 1.53–1.55 Ga, 1.34–1.37 Ga and 1.13–1.18 Ga ages Liu *et al.* (2017*c*). Our results show the zircon grains of 2.3–2.6 Ga and 1.7–2.0 Ga are commonly rounded and subhedral, suggesting they have undergone long distance or multi-cycled transport processes. The core part of some zircons shows clear oscillatory zoning, whereas the rim is dark without zoning (online Supplementary Material Fig. S1 (S7: b1; S8: b5) available at http://journals.cambridge.org/geo), which is considered to indicate reworked igneous zircons (Hoskin & Black, 2000; Hoskin & Schaltegger, 2003). Some zircons have misted textures and no clear zoning, with relatively flat LREE patterns, corresponding to metamorphic origins (online Supplementary Material Fig. S1 (S8: b1) available at http://journals.cambridge.org/geo). The zircons of 1.2–1.7 Ga age show a homogeneous texture or contrasting rim texture, indicative of metamorphic or hydrothermal reworked zircons (online Supplementary Material Fig. S1 (S7: c1–c3) available at http://journals.cambridge.org/geo). Grain b1 of sample S8 (1129 ± 32 Ma) exhibits a flat HREE pattern, suggesting coeval precipitation of zircon and garnet (Rubatto, 2002). The complicated zircons are consistent with the basement rocks of the North China Craton. Thus, we suggest the zircons of 2.3–2.6 Ga and 1.7–2.0 Ga ages are related to the basement rocks of the North China Craton.

In summary, the Upper Carboniferous to Lower Permian sandstones in the Mandula area accommodated the sediments derived from the basement rocks of the North China Craton, the Early to Middle Palaeozoic magmatic rocks of the Southern Orogenic Belt, and the syn-depositional volcanic rocks (260–330 Ma) in the tectonic units of the CAOB (e.g. the Solonker Belt and the Northern Orogenic Belt).

6.a.2. The Quagan Qulu area (the Shalazhashan Belt, close to the Nuru–Langshan Belt)

In the Quagan Qulu area, the stratigraphic age of the Amushan Formation was confirmed by the fusulinids of the *Pseudoschwagerina* Biozone (NMBGMR, 1991), but the sandstones of the Amushan Formation have a main zircon age group of 410–500 Ma and a subordinate group of 0.7–1.1 Ga, lacking the Late Palaeozoic zircons. The cross-bedding preserved in the sandstones indicates the palaeo-current directions are from the southeast to northwest, and thus the Nuru–Langshan Belt is a possible source. The lack of Late Palaeozoic zircons can be explained by the Permian plutons in the source area having not been uplifted and eroded at the time of deposition of the Amushan Formation, or the sandstones in the Quagan Qulu area represent a different lithotectonic unit.

Almost all the Early Palaeozoic zircons have clear or weak oscillatory zoning and typical REE patterns of magmatic zircons, yet several grains show homogeneous or patchy textures and relatively flat LREE patterns, indicative of metamorphic origins (online Supplementary Material Fig. S2 (WLJ-8: e6–e8, WLJ-5: e6) available at http://journals.cambridge.org/geo). The Early Palaeozoic magmatic zircons might derive from the Early Palaeozoic (410–460 Ma) arc-related granitic and dioritic rocks exposed in the Nuru–Langshan Belt owing to the Palaeo-Asian Ocean subduction Liu *et al.* (2017*a*). We speculate that the Early Palaeozoic metamorphic zircons are probably related to subduction/accretionary complexes, which are currently not exposed, or possibly hidden beneath the Mesozoic rocks in the Nuru–Langshan Belt.

The zircons of 0.7–1.0 Ga age are of magmatic types as suggested by the clear oscillatory zoning and typical REE patterns (Fig. 10). These zircons ages were reported in the volcanic layers of the Langshan group and the S-type granites in the Nuru–Langshan Belt (Dan *et al.* 2014*b*; Hu *et al.* 2014).

The basement rocks or metamorphic rocks in the Nuru–Langshan Belt are important source rocks, as

https://doi.org/10.1017/S0016756817000978 Published online by Cambridge University Press

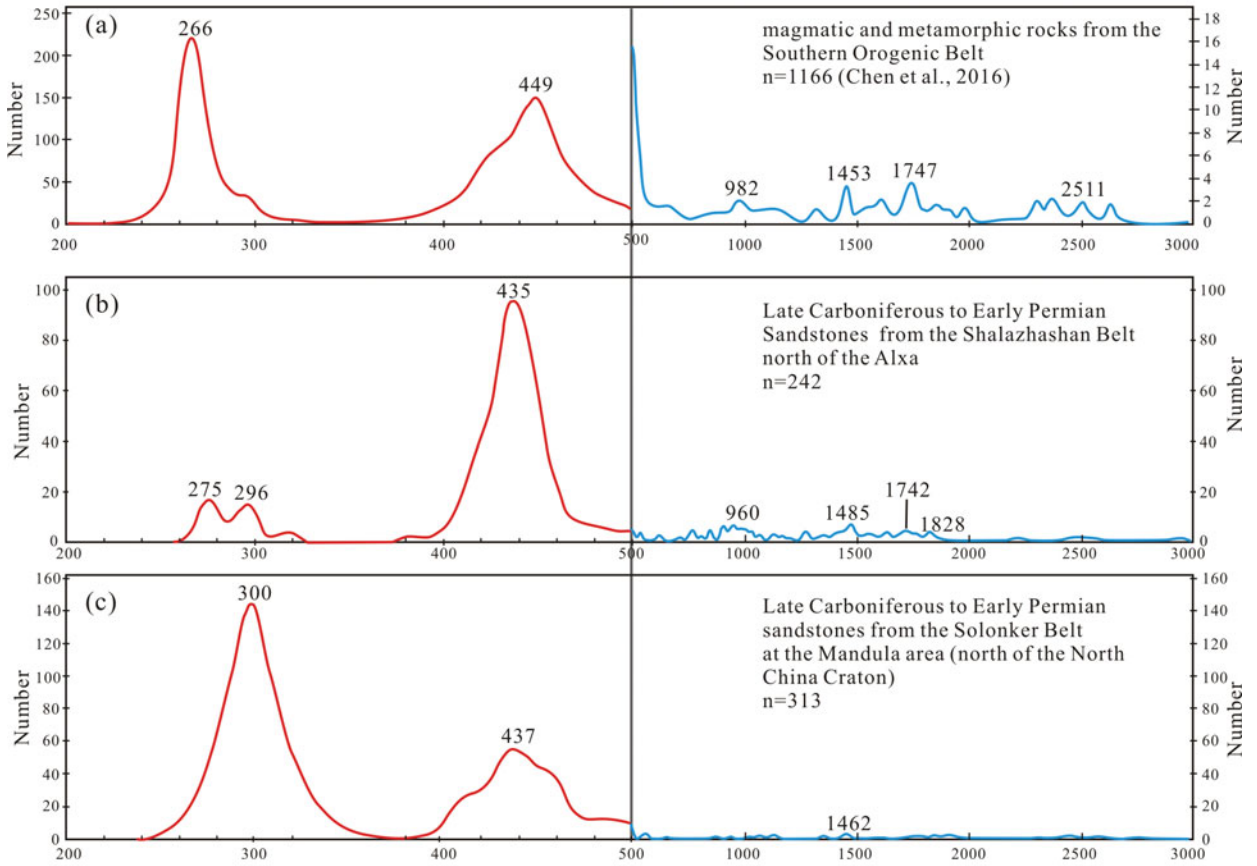

Figure 12. (Colour online) Comparison of the age spectra among the samples of the Shalazhashan Belt, the Solonker Belt and the potential source of the Southern Orogenic Belt. The data for the Southern Orogenic Belt and part of the zircons in the Mandula area are according to Chen, Zheng & Zhao (2016).

a significant amount of biotite, muscovite and garnet were found in the sandstones of the Amushan Formation (Shi *et al*. 2016). Some zircons of 1.0–1.1 Ga age have features of magmatic zircons, whereas a few zircons of 1.0–1.1 Ga age show distinct features of metamorphic zircons (online Supplementary Material Fig. S2 available at http://journals.cambridge.org/geo). These zircons and related rock types are not well known in the Nuru–Langshan Belt. The grains of 1.3–1.5 Ga, 1.7–1.9 Ga and ∼ 2.5 Ga ages are generally rounded and subhedral, a common feature of long distance or multi-cycle transportation. Some grains show relatively flat LREE patterns, and no or weakly positive Ce anomalies (e.g. WLJ-8: a1), representing the differences in source materials or subsequent metamorphism (Whitehouse & Platt, 2003). The complicated zircons could derive from the sedimentary rocks of the Neoproterozoic Langshan group which include similar age spectra (Hu *et al*. 2014), or directly derive from the basement rocks of the Nuru–Langshan Belt.

In summary, the Nuru–Langshan Belt is the source area for the Upper Carboniferous to Lower Permian sandstones. The source rocks include the Early Palaeozoic arc-related magmatic rocks, the magmatic rocks of 0.7–0.9 Ga age, and possibly the Neoproterozoic Langshan group and the Palaeoproterozoic, Archaean basement rocks.

6.a.3. The Enger Us area (the Shalazhashan Belt, close to the Zhusileng–Hangwula Belt (CAOB))

The zircons of 270–320 Ma age in the Enger Us area show oscillatory zoning and typical REE patterns of magmatic zircons. Moreover, the ε_{Hf} values are positive, plotting in the field of the CAOB (Fig. 11). This excludes the Nuru–Langshan Belt as the source area, as the Late Palaeozoic zircons of the Nuru–Langshan Belt have negative ε_{Hf} values, similar to that of the North China Craton (Geng & Zhou, 2012; Dan *et al*. 2014*a*, 2015). The Late Palaeozoic magmatic rocks are widely distributed in the Shalazhashan Belt and the Zhusileng–Hangwula Belt, and the magmatic rocks are characterized by positive zircon ε_{Hf} values (e.g. Shi *et al*. 2014). Considering the large proportion of volcanic fragments in the samples, the zircons of 270–320 Ma age should derive from the syndepositional volcanic rocks in the Shalazhashan Belt and the Zhusileng–Hangwula Belt.

The zircons of 410–500 Ma age are related to the Early Palaeozoic magmatic rocks in the Nuru–Langshan Belt. Most zircons of 410–500 Ma age have clear oscillatory zoning of igneous zircons and have negative ε_{Hf} values, which are consistent with the Early Palaeozoic zircons from the Nuru–Langshan Belt Liu *et al*. (2017*a*).

https://doi.org/10.1017/S0016756817000978 Published online by Cambridge University Press

Some zircons of 1.7–2.0 Ga age have the clear oscillatory zoning of igneous zircons, but some show dark homogeneous structures, or a light zoned inner core with dark rim, suggesting the zircons have undergone metamorphic reworking (online Supplementary Material Fig. S3 (WLJ-29-1: b3–b5) available at http://journals.cambridge.org/geo). The zircons of 1.4 Ga and 0.9–1.1 Ga ages, and some zircons of 1.5 Ga and 1.3 Ga ages have the weak or clear oscillatory zoning of igneous zircons, and all zircons of 1.6 Ga age and some zircons of 1.5 Ga and 1.3 Ga ages are homogeneous without zoning, or have a dark rim with light inner core (online Supplementary Material Fig. S3 (NJ-7: d1–d8) available at http://journals.cambridge.org/geo). Grain c6 of sample NJ-7 (1369 ± 32 Ma) has low LREE contents and Th/U ratio (< 0.10), indicating a metamorphic origin. The Precambrian rocks in the Zhusileng–Hangwula Belt and the Nuru–Langshan Belt contain zircons of 0.7–1.2 Ga and 1.2–1.7 Ga ages (NMBGMR, 1991; Wang *et al*. 2001; Zhou *et al.* 2013). Therefore, the Precambrian zircons in the Enger Us area could be from both the Zhusileng–Hangwula Belt and the Nuru–Langshan Belt.

In summary, the Nuru–Langshan Belt, the Shalazhashan Belt and the Zhusileng–Hangwula Belt are the source areas for the Upper Carboniferous to Permian sandstones in the Enger Us area. The Late Palaeozoic volcanic rocks of the Shalazhashan Belt and the Zhusileng–Hangwula Belt are the sources for the zircons of 270–320 Ma age, whereas the Early Palaeozoic magmatic rocks in the Nuru–Langshan Belt are responsible for the zircons of 410–500 Ma age.

6.b. Sedimentary environment and palaeogeographic reconstruction

6.b.1. Lithofacies interpretations

6.b.1.a. The Mandula area

We interpreted the olistostrome as representing slump deposits developed on intrabasinal topographic highs (e.g. horsts) or basin margin shoulders, such as carbonate platforms, because the original carbonate rocks are widespread in the Amushan Formation of the Southern Orogenic Belt. The amount and size of the limestone blocks decreases northwards, and the matrix of the olistostrome is made of brown greywacke in the south and dark grey mudstones in the north, indicating a northward slumping process.

The thick- to medium-bedded sandstone of the Baotege Formation and the conglomerate of the Zhesi Formation are considered as hyperconcentrated density flow or debris flow deposits related to the slumping event (e.g. Lowe, 1982; Mulder & Alexander, 2001). The thick- to medium-bedded sandstone is mainly distributed to the north of the olistostrome and probably represents the evolutional products of the slump deposits. The conglomerate of the Zhesi Formation is interpreted as debris flows that spread northwards over the turbidite, and the outsized limestone clasts were derived from limestone of the Amushan Formation. It appears to represent relatively short-term 'catastrophic' events related to major slides.

The sandstone–mudstone couplets (laminae) are interpreted as submarine fan lobe deposits in a turbidite system (e.g. Lowey, 2007). Based on the fine grain size and lamination, the turbidite is interpreted to have been deposited in low-energy, deep-water environments.

6.b.1.b. The Quagan Qulu and Enger Us areas

The middle member of thick- to medium-bedded limestone represents a carbonate platform (e.g. Bu *et al.* 2012). As in the upper member of the Amushan Formation, the lower thick-bedded pebbly sandstone and coarse sandstone with cross-stratification are interpreted to represent neritic sea sedimentation within a high-energy environment; the upper fine-grained strata have a significant amount of mudstone and turbidite Tde divisions, which are interpreted as having been deposited in a deep basinal position within a relatively low-energy environment. The fine-grained succession in the Enger Us area represents deep-water environments of low energy and short of sand supply.

6.b.2. Sedimentary environment

The Late Palaeozoic sedimentary environments in western Inner Mongolia were intensively studied, but no consensus has been reached, because of the poor outcrops and the lack of precise stratigraphic ages (Shen *et al.* 2006). The Upper Carboniferous to Permian sediments are generally deposited in shallow-marine environments (Mueller *et al*. 1991; Shen *et al.* 2006; Li, Lu & Chen, 2011; Bu *et al.* 2012; Li *et al*. 2012), though a deep-water environment was suggested according to the radiolarian fauna found in the mudstone of the Middle Permian strata (Shang, 2004). Shao, Tang & He (2014) studied the Lower Permian strata in central Inner Mongolia and observed an upward-deepening sedimentary succession, and Li, Lu & Chen (2011) argued that the Amushan Formation in western Inner Mongolia has undergone a transition from terrestrial to shallow-marine deposition.

For our field observations, the lithological assemblages of shallow-marine environments are mainly distributed in the Southern Orogenic Belt and the southern part of the Shalazhashan Belt (e.g. the Quagan Qulu area). The lithological assemblages indicating deep-water environments are mostly distributed in part of the Solonker Belt and the northern part of the Shalazhashan Belt (e.g. the Enger Us area). The transitional zone between the shallow- and deep-water environments often develops slump deposits (Fig. 13).

In the Mandula area, the Amushan Formation in the Southern Orogenic Belt is composed of shallow-marine sediments characterized by lithological assemblages of reef limestone, sandstones and volcanic rocks, including fossils of brachiopods, corals, ammonoids and fusulinids (NMBGMR, 1991; Yang

https://doi.org/10.1017/S0016756817000978 Published online by Cambridge University Press

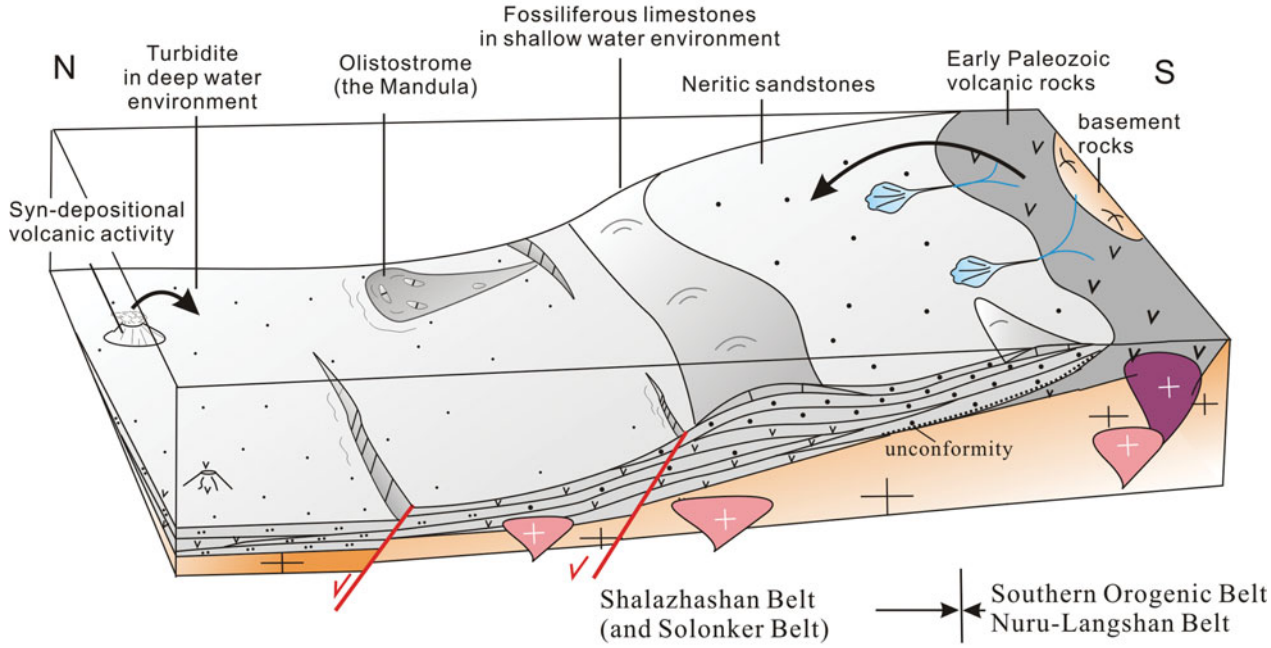

Figure 13. (Colour online) Sedimentary environments and palaeogeographic reconstruction of western Inner Mongolia.

et al. 2015). Northwards, the olistostromes represent the slump deposits developed in the transition zone from the shallow-marine to deep-water environments. Further north, the Baotege Formation is characterized by thin-bedded sandstone and mudstone (or silicified mudstone) couplets which contain radiolarian faunas, suggesting deep-water environments (Wang *et al.* 2005). The Dashizhai Formation, characterized by the mudstones, siltstones and intercalations of volcanic and volcaniclastic rocks, represents volcanic eruption-related deposits in submarine environments (NMBGMR, 1991, Jiang *et al.* 1995). Therefore, we argue for generally northward-deepening environments.

The detrital zircon analyses also support the presence of northward-deepening sedimentary environments (Fig. 13). The Upper Palaeozoic sandstones in the Southern Orogenic Belt (shallow-marine environment) mainly accommodated the terrestrial clasts from the North China Craton and the Southern Orogenic Belt (Yang *et al.* 2015; Chen, Zheng & Zhao, 2016; Zhang & Zhang, 2016). By contrast, the sandstones in the Solonker Belt (partly in deep-water environments) accommodated sediments from the North China Craton and the Southern Orogenic Belt, and also the Solonker Belt and the Northern Orogenic Belt.

The sedimentary rocks in the Shalazhashan Belt also demonstrate similar environments of northward deepening. The Amushan Formation in the Quagan Qulu area has lithological assemblages of thick-bedded sandstones and limestones, develops cross-bedding sedimentary structures, and contains fossils of brachiopods, corals, ammonoids and fusulinids, suggesting shallow-marine environments (Han *et al.* 2012; Shi *et al.* 2016). In contrast, the sedimentary formations in the Enger Us area are characterized by rhythmic beds of siltstone and silicified mudstone, and thin-bedded volcanic and volcaniclastic rocks deposited in relatively deep-water environments. Radiolarian faunas are also found in the Enger Us area (Xie *et al.* 2014).

Our provenance analyses in the Shalazhashan Belt are also consistent with the presence of northward-deepening environments. The sediments in the Quagan Qulu area (shallow-water environment) derive from the Nuru–Langshan Belt to the south. However, the sediments in the Enger Us area (deep-water environment) derive from the Nuru–Langshan Belt to the south, and the Shalazhashan Belt and the Zhusileng–Hangwula Belt to the north.

6.b.3. Palaeogeographic reconstruction

We consider the Shalazhashan Belt to be the western extension of the Solonker Belt, because the Shalazhashan Belt and the Solonker Belt share similar detrital age spectra (Fig. 12). The Nuru–Langshan Belt was involved in the Early Palaeozoic Palaeo-Asian Ocean subduction event, the same as the Southern Orogenic Belt Liu *et al.* (2017*a*). The palaeogeomagnetic and structural evidence also suggested that the Alxa block southwardly migrated along the Langshan fault relative to the North China Craton after Permian time (Zhang *et al.* 2013*a*; Yuan & Yang, 2015). When the Alxa block is restored to its initial position, the Southern Orogenic Belt and the Solonker Belt are parallel to the Nuru–Langshan Belt and the Shalazhashan Belt, respectively.

Our detrital zircons include a main age group of 410–500 Ma, suggesting that the Early Palaeozoic arc-related magmatic rocks in the Southern Orogenic Belt and the Nuru–Langshan Belt were uplifted to become erosion areas in Late Palaeozoic time (Fig. 13).

https://doi.org/10.1017/S0016756817000978 Published online by Cambridge University Press

Meanwhile, in the deep-water environments, the Late Palaeozoic calc-alkaline volcanic rocks were active in the Solonker Belt and the Shalazhashan Belt (Zhang *et al.* 2008, 2017; Chen *et al.* 2012; Shi *et al.* 2014; Shao, Tang & He, 2014), which provided the detrital zircons of 260–330 Ma age. The palaeogeography might be characterized by relatively high-relief landscapes or slope areas for the development of olistostromes (Fig. 13).

6.c. Tectonic setting

Some researchers suggested the northern margin of the Alxa block can be ascribed to a subduction setting during Late Carboniferous to Early Permian times (Shi *et al.* 2012*b*; Feng *et al.* 2013; Peng *et al.* 2013; Lin *et al.* 2014; Wang *et al.* 2015; Liu *et al.* 2017*b*). The Late Permian magmatic rocks in the Shalazhashan Belt, characterized by high-K calc-alkaline, peraluminous granitoids, are produced in extensional regimes (Zhang *et al.* 2013*b*; Lin *et al.* 2014; Shi *et al.* 2014). Our field observations show there is a generally northward-deepening sedimentary environment in the northern margins of the Alxa and the North China Craton. Such an upward-fining sequence is common both in foreland basins and extensional basins. We consider that extensional basins are more likely, because large volumes of high-K calc-alkaline Permian granites and N-MORB-like basalts occurred in the Shalazhashan Belt (Shi *et al.* 2014; Zheng *et al.* 2014). The provenance and sedimentary environments of the Amushan Formation are consistent with the extensional setting. According to the tectonic scenario of the subduction settings (e.g. Zheng *et al.* 2014; Li *et al.* 2014, 2017*b*; Liu *et al.* 2017*b*), the extensional basins were developed in fore-arc settings. However, extensional basins in rifting settings cannot be excluded. Dan *et al*. (2014*a*, 2015) argued that the magma flare-up at *c*. 280 Ma was in an extensional setting and triggered by the Tarim mantle plume. The Solonker ultramafic rocks are Ligurian-type ones (Xu *et al.* 2014; Luo *et al.* 2016; Pang *et al*. 2016). The volcanic rocks of the Dashizhai Formation have bimodal characteristics, corresponding to rift-related magmatism (Zhang *et al*. 2008, 2017; Shao, Tang & He, 2014). Our detrital zircons show a large age gap between 340 and 400 Ma (Fig. 12), indicating a silent magmatic period. After the Early Carboniferous period of magmatic quiescence, the CAOB in western Inner Mongolia entered stages of extension. But, to verify a subduction or rifting setting needs more reliable evidence to further explore it. The detrital zircons show Hf model ages in a large range of 0.8–1.8 Ga, with a dominant population of 1.0–1.5 Ga, which suggests that protoliths of 1.0–1.5 Ga or earlier have participated in the precipitation of zircon. Moreover, mixing of the ancient lower crust and juvenile materials is necessary to produce the large range of model ages in the Early and Late Palaeozoic magmatism.

7. Conclusion

Based on our new petrographic, zircon morphology, and U–Pb and Hf isotopic data, along with previous studies, we may draw the following conclusions:

(a) The Upper Palaeozoic sandstones in the Shalazhashan Belt and the Solonker Belt have similar detrital zircon spectra. The zircons have two main sources: (i) the Early Palaeozoic arc-related magmatic rocks in the Southern Orogenic Belt and the Nuru–Langshan Belt, and (ii) the Late Palaeozoic syn-depositional volcanic rocks in the tectonic units of the CAOB (e.g. the Solonker Belt and the Shalazhashan Belt). The surrounding and internal Precambrian cratons/terranes might be the subordinate sources.

(b) The Upper Palaeozoic sandstones (the Amushan Formation) in western Inner Mongolia were deposited in shallow-marine to deep-water environments, with a northward-deepening transition. The sedimentary environment and provenance are consistent with extensional settings developed in the Early Palaeozoic orogens.

Acknowledgements. This study was supported by the National Natural Science Foundation of China (No. 41402192) and the China Postdoctoral Science Foundation (No. 2014M562080).

Supplementary material

To view supplementary material for this article, please visit https://doi.org/10.1017/S0016756817000978

References

Andersen, T. 2005. Detrital zircons as tracers of sedimentary provenance: limiting conditions from statistics and numerical simulation. *Chemical Geology* **216**, 249–70.

Badarch, G., Cunningham, W. D. & Windley, B. F. 2002. A new terrane subdivision for Mongolia: implications for the Phanerozoic crustal growth of central Asia. *Journal of Asian Earth Sciences* **21**, 87–110.

Belousova, E. A., Griffin, W. L., O'Reilly, S. Y. & Fisher, N. I. 2002. Igneous zircon: trace element composition as an indicator of source rock type. *Contributions to Mineralogy and Petrology* **143**, 602–22.

BGIM (Bureau of Geology of Inner Mongolia). 2004. *Geological Map of 1/250 000 in Mandula Region*. (in Chinese).

Blichert-Toft, J. & Albarede, F. 1997. The Lu–Hf isotope geochemistry of chondrites and the evolution of the mantle–crust system. *Earth and Planetary Science Letters* **148**, 243–58.

Bu, J. J., Niu, Z. J., Wu, J. & Duan, X. F. 2012. Sedimentary characteristics and age of Amushan Formation in Ejin Banner and its adjacent areas, western Inner Mongolia. *Geological Bulletin of China* **31**, 1669–83.

Bouma, A. H. 1962. *Sedimentology of Some Flysch Deposits*. Amsterdam: Elsevier, 168 pp.

Charvet, J., Shu, L. S., Laurent-Charvet, S., Wang, B., Faure, M., Cluzel, D., Chen, Y. & De Jong, K. 2011. Palaeozoic tectonic evolution of the Tianshan belt, NW China. *Science China: Earth Sciences* **54**, 166–84.

Chen, B., Jahn, B. M., Wilde, S. & Xu, B. 2000. Two contrasting Paleozoic magmatic belts in northern Inner Mongolia, China: petrogenesis and tectonic implications. *Tectonophysics* **328**, 157–82.

Chen, C., Zhang, Z. C., Guo, Z. J., Li, J. F., Feng, Z. S. & Tang, W. H. 2012. Geochronology, geochemistry, and its geological significance of the Permian Mandula mafic rocks in Damaoqi, Inner Mongolia. *Science China: Earth Sciences* **55**, 39–52.

Chen, C., Zhang, Z. C., Li, K., Chen, Y., Tang, W. H. & Li, J. F. 2015. Geochronology, geochemistry, and its geological significance of the Damaoqi Permian volcanic sequences on the northern margin of the North China Block. *Journal of Asian Earth Sciences* **97**, 307–19.

Chen, L., Zheng, Y. F. & Zhao, Z. F. 2016. Geochemical constraints on the origin of Late Mesozoic andesites from the Ningwu basin in the Middle–Lower Yangtze Valley, South China. *Lithos* **254–255**, 94–117.

Choulet, F., Chen, Y., Cogné, J. P., Rabillard, A., Wang, B., Lin, W., Faure, M. & Cluzel, D. 2013. First Triassic palaeomagnetic constraints from Junggar (NW China) and their implications for the Mesozoic tectonics in Central Asia. *Journal of Asian Earth Sciences* **78**, 371–94.

Choulet, F., Cluzel, D., Faure, M., Lin, W., Wang, B., Chen, Y., Wu, F. Y. & Ji, W. B. 2012a. New constraints on the pre-Permian continental crust growth of Central Asia (West Junggar, China) by U–Pb and Hf isotopic data from detrital zircon. *Terra Nova* **24**, 189–98.

Choulet, F., Faure, M., Cluzel, D., Lin, W., Wang, B. & Jahn, B. M. 2012b. Architecture and evolution of accretionary orogens in the Altaids collage: the early Paleozoic West Junggar (NW China). *American Journal of Science* **312**, 1098–145.

Chu, H., Zhang, J. R., Wei, C. J., Wang, H. & Ren, Y. 2013. A new interpretation of the tectonic setting and age of meta-basic volcanics in the Ondor Sum Group, Inner Mongolia. *China Science Bulletin* **58**, 3580–7.

Corfu, F., Hanchar, J. M., Hoskin, P. W. & Kinny, P. 2003. Atlas of zircon textures. *Reviews in Mineralogy and Geochemistry* **53**, 469–500.

Dan, W., Li, X.-H., Guo, J. H., Liu, Y. & Wang, X. C. 2012. Paleoproterozoic evolution of the eastern Alxa Block, westernmost North China: evidence from in situ zircon U–Pb dating and Hf–O isotopes. *Gondwana Research* **21**, 838–64.

Dan, W., Li, X. H., Wang, Q., Tang, G. J. & Liu, Y. 2014a. An Early Permian (ca. 280 Ma) silicic igneous province in the Alxa Block, NW China: a magmatic flare-up triggered by a mantle-plume? *Lithos* **204**, 144–58.

Dan, W., Li, X. H., Wang, Q., Wang, X. C. & Liu, Y. 2014b. Neoproterozoic S-type granites in the Alxa block, westernmost north China and tectonic implications: in situ zircon U–Pb–Hf–O isotopic and geochemical constraints. *American Journal of Science* **314**, 110–53.

Dan, W., Wang, Q., Wang, X. C., Liu, Y., Wyman, D. A. & Liu, Y.-S. 2015. Overlapping Sr–Nd–Hf–O isotopic compositions in Permian mafic enclaves and host granitoids in Alxa Block, NW China: evidence for crust-mantle interaction and implications for the generation of silicic igneous provinces. *Lithos* **230**, 133–45.

Dickinson, W. R. 1985. Interpreting provenance relations from detrital modes of sandstones. In *Provenance of Arenites* (ed. G. G. Zuffa), pp. 333–61. NATO Science Series 148.

Dodson, M. H., Compston, W., Williams, I. S. & Wilson, J. F. 1988. A search for ancient detrital zircons in Zimbabwean sediments. *Journal of the Geological Society, London* **145**, 977–83.

Eizenhöfer, P. R., Zhao, G. C., Sun, M., Zhang, J., Han, Y. G. & Hou, W. Z. 2015a. Geochronological and Hf isotopic variability of detrital zircons in Paleozoic strata across the accretionary collision zone between the North China craton and Mongolian arcs and tectonic implications. *Geological Society of America Bulletin* **127**, 1422–36.

Eizenhöfer, P. R., Zhao, G. C., Zhang, J., Han, Y. G., Hou, W. Z., Liu, D. X. & Wang, B. 2015b. Geochemical characteristics of the Permian basins and their provenances across the Solonker Suture Zone: assessment of net crustal growth during the closure of the Palaeo-Asian Ocean. *Lithos* **224**, 240–55.

Eizenhöfer, P. R., Zhao, G. C., Zhang, J. & Sun, M. 2014. Final closure of the Paleo-Asian Ocean along the Solonker Suture Zone: constraints from geochronological and geochemical data of Permian volcanic and sedimentary rocks. *Tectonics* **33**, 441–63.

Fan, H. R., Hu, F. F., Yang, K. F., Pirajno, F., Liu, X. & Wang, K. Y. 2014. Integrated U–Pb and Sm–Nd geochronology for a REE-rich carbonatite dyke at the giant Bayan Obo REE deposit, Northern China. *Ore Geology Reviews* **63**, 510–9.

Fan, H. R., Yang, K. F., Hu, F. F., Wang, K. Y. & Zhai, M. G. 2010. Zircon geochronology of basement rocks from the Bayan Obo area, Inner Mongolia, and tectonic implications. *Acta Petrologica Sinica* **26**, 1342–50 (in Chinese with English abstract).

Feng, J. Y., Xiao, W. J., Windley, B., Han, C. M., Wan, B., Zhang, J. E., Ao, S. J., Zhang, Z. Y. & Lin, L. N. 2013. Field geology, geochronology and geochemistry of mafic-ultramafic rocks from Alxa, China: implications for Late Permian accretionary tectonics in the southern Altaids. *Journal of Asian Earth Sciences* **78**, 114–42.

Geng, Y. S., Wang, X. S., Shen, Q. H. & Wu, C. M. 2007. Chronology of the Precambrian metamorphic series in the Alxa area, Inner Mongolia. *Geology in China* **34**, 251–61 (in Chinese with English abstract).

Geng, Y. S. & Zhou, X. W. 2010. Early Neoproterozoic granite events in Alxa area of Inner Mongolia and their geological significance: evidence from geochronology. *Acta Petrologica et Mineralogica* **29**, 779–95 (in Chinese with English abstract).

Geng, Y. S. & Zhou, X. W. 2012. Early Permian magmatic events in the Alxa metamorphic basement: evidence from geochronology. *Acta Petrologica Sinica* **28**, 2667–85.

Griffin, W. L., Belousova, E. A., Shee, S. R., Pearson, N. J. & O'Reilly, S. Y. 2004. Archean crustal evolution in the northern Yilgarn Craton: U–Pb and Hf-isotope evidence from detrital zircons. *Precambrian Research* **131**, 231–82.

Han, W., Liu, X., Li, J. C. & Shi, J. Z. 2012. Sedimentary environment of Carboniferous–Permian Amushan Formation in Wulanaobao area of Urad Rear Banner, Inner Mongolia. *Geological Bulletin of China* **31**, 1684–91.

Hoskin, P. & Black, L. 2000. Metamorphic zircon formation by solid-state recrystallization of protolith igneous zircon. *Journal of Metamorphic Geology* **18**, 423–39.

Hoskin, P. W. & Ireland, T. R. 2000. Rare earth element chemistry of zircon and its use as a provenance indicator. *Geology* **28**, 627–30.

Hoskin, P. W. & Schaltegger, U. 2003. The composition of zircon and igneous and metamorphic petrogenesis. *Reviews in Mineralogy and Geochemistry* **53**, 27–62.

Hu, J. M., Gong, W. B., Wu, S. J., Liu, Y. & Liu, S. C. 2014. LA-ICP-MS zircon U–Pb dating of the Langshan Group in the northeast margin of the Alxa block, with tectonic implications. *Precambrian Research* **255**, 756–70.

Hu, C. S., Li, W. B., Xu, C., Zhong, R. C. & Zhu, F. 2015. Geochemistry and zircon U–Pb–Hf isotopes of the granitoids of Baolidao and Halatu plutons in Sonidzuoqi area, Inner Mongolia: implications for petrogenesis and geodynamic setting. *Journal of Asian Earth Sciences* **97**, 294–306.

Hu, Z. C., Liu, Y. S., Gao, S., Liu, W. G., Yang, L., Zhang, W., Tong, X. R., Lin, L., Zong, K. Q., Li, M., Chen, H. H., Zhou, L. & Yang, L. 2012. Improved in situ Hf isotope ratio analysis of zircon using newly designed X skimmer cone and Jet sample cone in combination with the addition of nitrogen by laser ablation multiple collector ICP-MS. *Journal of Analytical Atomic Spectrometry* **27**, 1391–9.

Ingersoll, R. V., Bullard, T. F., Ford, R. L., Pickle, J. D. & Sares, S. W. 1984. The effect of grain size on detrital modes: a test of the Gazzi–Dickinson point-counting method. *Journal of Sedimentary Research* **54**, 103–6.

Jahn, B. M. 2004. The Central Asian Orogenic Belt and growth of the continental crust in the Phanerozoic. In *Aspects of the Tectonic Evolution of China* (eds J. Malpas, C. J. N. Fletcher, J. R. Ali & J. C. Aitchison), pp. 73–100. Geological Society of London, Special Publication no. 226.

Jahn, B. M., Capdevila, R., Liu, D. Y., Vernon, A. & Badarch, G. 2004. Sources of Phanerozoic granitoids in the transect Bayanhongor-Ulaan Baatar, Mongolia: geochemical and Nd isotopic evidence, and implications for Phanerozoic crustal growth. *Journal of Asian Earth Sciences* **23**, 629–53.

Jian, P., Liu, D. Y., Kröner, A., Windley, B. F., Shi, Y. R., Zhang, F. Q., Shi, G. H., Miao, L. C., Zhang, W., Zhang, Q., Zhang, L. Q. & Ren, J. S. 2008. Time scale of an early to mid-Paleozoic orogenic cycle of the long-lived Central Asian Orogenic Belt, Inner Mongolia of China: implications for continental growth. *Lithos* **101**, 233–59.

Jian, P., Liu, D. Y., Kröner, A., Windley, B. F., Shi, Y. R., Zhang, W., Zhang, F. Q., Miao, L. C., Zhang, L. Q. & Tomurhuu, D., 2010. Evolution of a Permian intraoceanic arc–trench system in the Solonker suture zone, Central Asian Orogenic Belt, China and Mongolia. *Lithos* **118**, 169–90.

Jiang, G. Q., Xu, Y. K., Zhao, G. C., Luo, F., Xiao, R. G. & Luo, Z. H. 1995. Evolution of process-facies and environment-facies sequence of Permian Dashizhai Formation in Sonid Zuoqi area, Inner Mongolia. *Geoscience* **9**, 170–8 (in Chinese with English abstract).

Kröner, A., Kovach, V., Belousova, E., Hegner, E., Armstrong, R., Dolgopolova, A., Seltmann, R., Alexeiev, D. V., Hoffmann, J. E., Wong, J., Sun, M., Cai, K., Wang, T., Tong, Y., Wilde, S. A., Degtyarev, K. E. & Rytsk, E. 2014. Reassessment of continental growth during the accretionary history of the Central Asian Orogenic Belt. *Gondwana Research* **25**, 103–25.

Li, J. J. 2006. *Regional Metallogenic System of Alxa Block in Inner Mongolia Autonomous Region [D]*. Beijing: China University of Geosciences.

Li, W., Bai, R., Niu, Y. Z. & Chen, G. C. 2012. Sedimentary environments of the Permian Haersuhai Formation in Yagan area, Ejin Banner, western Inner Mongolia. *Geological Bulletin of China* **31**, 1703–14.

Li, Y.-L., Brouwer, F. M., Xiao, W.-J. & Zheng, J.-P. 2017a. Late Devonian to Early Carboniferous arc-related magmatism in the Baolidao arc, Inner Mongolia, China: significance for southward accretion of the eastern Central Asian orogenic belt. *Geological Society of America Bulletin* **129**, 677–97.

Li, Y.-L., Brouwer, F. M., Xiao, W.-J. & Zheng, J.-P. 2017b. A Paleozoic fore-arc complex in the eastern Central Asian Orogenic Belt: petrology, geochemistry and zircon U–Pb–Hf isotopic composition of paragneisses from the Xilingol Complex in Inner Mongolia, China. *Gondwana Research* **47**, 323–41.

Li, D. P., Chen, Y. L., Wang, Z., Hou, K. J. & Liu, C. Z. 2011. Detrital zircon U–Pb ages, Hf isotopes and tectonic implications for Paleozoic sedimentary rocks from the Xing-Meng Orogenic Belt, middle-east part of Inner Mongolia, China. *Geological Journal* **46**, 63–81.

Li, W., Lu, J. C. & Chen, G. C. 2011. Sedimentary environment of Carboniferous–Permian strata in Ejin Banner and its vicinities, western Inner Mongolia. *Geological Bulletin of China* **30**, 983–92.

Li, Y. L., Zhou, H. W., Brouwer, F. M., Xiao, W. J., Wijbrans, J. R. & Zhong, Z. Q. 2014. Early Paleozoic to Middle Triassic bivergent accretion in the Central Asian Orogenic Belt: insights from zircon U–Pb dating of ductile shear zones in central Inner Mongolia, China. *Lithos* **205**, 84–111.

Lin, J., Liu, Y. S., Chen, H. H., Zhou, L., Hu, Z. C. & Gao, S. 2015. Review of high-precision Sr isotope analyses of low-Sr geological samples. *Journal of Earth Science* **26**, 763–74.

Lin, L. N., Xiao, W. J., Wan, B., Windley, B. F., Ao, S. J., Han, C. M., Feng, J. Y., Zhang, J. E. & Zhang, Z. Y. 2014. Geochronology and geological evidence for persistence of south-dipping subduction to Late Permian time, Langshan area, Inner Mongolia (China): significance for termination of accretionary orogenesis in the southern Altaids. *American Journal of Science* **314**, 679–703.

Liu, Y. S., Gao, S., Hu, Z. C., Gao, C. G., Zong, K. Q. & Wang, D. B. 2010. Continental and oceanic crust recycling-induced melt-peridotite interactions in the Trans-North China Orogen: U–Pb dating, Hf isotopes and trace elements in zircons from mantle xenoliths. *Journal of Petrology* **51**, 537–71.

Liu, Y. S., Hu, Z. C., Gao, S., Günther, D., Xu, J., Gao, C. G. & Chen, H. H. 2008. In situ analysis of major and trace elements of anhydrous minerals by LA-ICP-MS without applying an internal standard. *Chemical Geology* **257**, 34–43.

Liu, Y. J., Li, W. M., Feng, Z. Q., Wen, Q. B., Neubauer, F. & Liang, C. Y. 2017a. A review of the Paleozoic tectonics in the eastern part of Central Asian Orogenic Belt. *Gondwana Research* **43**, 123–48.

Liu, J., Li, Y., Ling, M. X. & Sun, W. D. 2011. Chronology and geological significance of the basement rock of the giant Bayan Obo REE–Nb–Fe ore deposit. *Geochimica* **40**, 209–22.

Liu, Q., Zhao, G. C., Han, Y. G., Eizenhöfer, P. R., Zhu, Y. L., Hou, W. Z. & Zhang, X. R. 2017b. Timing of the final closure of the Paleo-Asian Ocean in the Alxa Terrane: constraints from geochronology and geochemistry of Late Carboniferous to Permian gabbros and diorites. *Lithos* **274–275**, 19–30.

Liu, C. H., Zhao, G. C., Liu, F. L. & Shi, J. R. 2017c. Detrital zircon U–Pb and Hf isotopic and whole-rock geochemical study of the Bayan Obo Group, northern margin of the North China Craton: implications for

Rodinia reconstruction. *Precambrian Research*, published online 28 April 2017. doi: 10.1016/j.precamres.2017.04.033.

Lowe, D. R. 1982. Sediment gravity flows; II, depositional models with special reference to the deposits of high-density turbidity currents. *Journal of Sedimentary Petrology* **52**, 279–97.

Lowey, G. W. 2007. Lithofacies analysis of the Dezadeash Formation (Jura–Cretaceous), Yukon, Canada: the depositional architecture of a mud/sand-rich turbidite system. *Sedimentary Geology* **198**, 273–91.

Ludwig, K. R. 2003. *Isoplot 3.00: A Geochronological Toolkit for Microsoft Excel*. Berkeley Geochronology Center, Special Publication no. 5.

Luo, Z. W., Xu, B., Shi, G. Z., Zhao, P., Faure, M. & Chen, Y. 2016. Solonker ophiolite in Inner Mongolia, China: a late Permian continental margin-type ophiolite. *Lithos* **261**, 72–91.

Mossakovsky, A. A., Ruzhentsev, S. V., Samygin, S. G. & Kheraskova, T. N. 1993. The Central Asian fold belt: geodynamic evolution and formation history. *Geotectonics* **26**, 455–73.

Mueller, J. F., Rogers, J. J. W., Jin, Y. G., Wang, H. Y., Li, W. G., Chronic, J., Mueller & Joseph, F. 1991. Late Carboniferous to Permian sedimentation in Inner Mongolia, China, and tectonic relationships between North China and Siberia. *Journal of Geology* **99**, 251–63.

Mulder, T. & Alexander, J. 2001. The physical character of subaqueous sedimentary density flows and their deposits. *Sedimentology* **48**, 269–99.

NMBGMR (Nei Mongol Bureau of Geology and Mineral Resources). 1991. *Regional Geology of Nei Mongol Autonomous Region*. Beijing: Geological Publishing House.

Pang, C. J., Wang, X. C., Xu, B., Luo, Z. W. & Liu, Y. Z. 2017. Hydrous parental magmas of Early to Middle Permian gabbroic intrusions in western Inner Mongolia, North China: new constraints on deep-Earth fluid cycling in the Central Asian Orogenic Belt. *Journal of Asian Earth Sciences* **144**, 184–204.

Pang, C. J., Wang, X. C., Xu, B., Zhao, J. X., Feng, Y. X., Wang, Y. Y., Luo, Z. W. & Liao, W. 2016. Late Carboniferous N-MORB-type basalts in central Inner Mongolia, China: products of hydrous melting in an intraplate setting? *Lithos* **261**, 55–71.

Peng, R. M., Zhai, Y. S., Li, C. S. & Ripley, E. M. 2013. The Erbutu Ni–Cu deposit in the Central Asian Orogenic Belt: a Permian magmatic sulfide deposit related to boninitic magmatism in an arc setting. *Economic Geology* **108**, 1879–88.

Rojas-Agramonte, Y., Kröner, A., Alexeiev, D. V., Jeffreys, T., Khudoley, A. K., Wong, J., Geng, H., Shu, L., Semiletkin, S. A., Mikolaichuk, A. V., Kiselev, V. V., Yang, J. & Seltmann, R. 2014. Detrital and igneous zircon ages for supracrustal rocks of the Kyrgyz Tianshan and palaeogeographic implications. *Gondwana Research* **26**, 957–74.

Rubatto, D. 2002. Zircon trace element geochemistry: partitioning with garnet and the link between U–Pb ages and metamorphism. *Chemical Geology* **184**, 123–38.

Sengör, A. M. C., Natal'in, B. A. & Burtman, V. S. 1993. Evolution of the Altaid tectonic collage and Paleozoic crustal growth in Eurasia. *Nature* **364**, 299–307.

Shang, Q. H. 2004. Occurrences of Permian radiolarians in central and Eastern Nei Mongol (Inner Mongolia) and their geological significance to the Northern China Orogen. *Chinese Science Bulletin* **49**, 2613–9.

Shao, J. A. 1991. *Crustal Evolution in the Middle Part of the Northern Margin of the Sino-Korean Plate*. Beijing: Peking University Publishing House (in Chinese with English abstract).

Shao, J. A., Tang, K. D. & He, G. Q. 2014. Early Permian tectono-palaeogeographic reconstruction of Inner Mongolia, China. *Acta Petrologica Sinica* **30**, 1858–66 (in Chinese with English abstract).

Shen, S. Z., Zhang, H., Shang, Q. H. & Li, W. Z. 2006. Permian stratigraphy and correlation of Northeast China: a review. *Journal of Asian Earth Sciences* **26**, 304–26.

Shi, G. Z., Faure, M., Xu, B., Zhao, P., Chen, Y. 2013. Structural and kinematic analysis of the Early Paleozoic Ondor Sum-Hongqi mélange belt, eastern part of the Altaids (CAOB) in Inner Mongolia, China. *Journal of Asian Earth Sciences* **66**, 123–39.

Shi, Y. R., Liu, D. Y., Kröner, A., Jian, P., Miao, L. C. & Zhang, F. Q. 2012a. Ca. 1318 Ma A-type granite on the northern margin of the North China Craton: implications for intraplate extension of the Columbia supercontinent. *Lithos* **148**, 1–9.

Shi, G. Z., Song, G. Z., Wang, H., Huang, C. Y., Zhang, L. D. & Tang, J. R. 2016. Late Paleozoic tectonics of the Wuliji area in the Solonker Zone: insights from stratigraphic sequence, chronological, and sandstone geochemistry analysis. *Journal of Asian Earth Sciences* **127**, 100–18.

Shi, X. J., Tong, Y., Wang, T., Zhang, J. J., Zhang, Z. C., Zhang, L., Guo, L., Zeng, T. & Geng, J. Z. 2012b. LA-ICP-MS zircon U–Pb age and geochemistry of the Early Permian Halinudeng granite in northern Alxa area, western Inner Mongolia. *Geological Bulletin of China* **31**, 662–70 (in Chinese with English abstract).

Shi, X. J., Wang, T., Zhang, L., Castro, A., Xiao, X. C., Tong, Y., Zhang, J. J., Guo, L. & Yang, Q. D. 2014. Timing, petrogenesis and tectonic setting of the Late Paleozoic gabbro–granodiorite–granite intrusions in the Shalazhashan of northern Alxa: constraints on the southernmost boundary of the Central Asian Orogenic Belt. *Lithos* **208–209**, 158–77.

Sun, S. S. & McDonough, W. F. 1989. Chemical and isotopic systematics of oceanic basalts: implications for mantle composition and processes. In *Magmatism in the Ocean Basins* (eds A. D. Saunders & M. J. Norry), pp. 313–45. Geological Society of London, Special Publication no. 42.

Tang, K. 1990. Tectonic development of Paleozoic fold belts at the north margin of the Sino-Korean craton. *Tectonics* **9**, 249–60.

Tong, Y., Hong, D. W., Wang, T., Shi, X. J., Zhang, J. J. & Zeng, T. 2010. Spatial and temporal distribution of granitoids in the middle segment of the Sino-Mongolian border and its tectonic and metallogenic implications. *Acta Geoscientica Sinica* **31**, 395–412 (in Chinese with English abstract).

Wang, Z. Z., Han, B. F., Feng, L. X. & Liu, B. 2015. Geochronology, geochemistry and origins of the Paleozoic–Triassic plutons in the Langshan area, western Inner Mongolia, China. *Journal of Asian Earth Sciences* **97**, 337–51.

Wang, Q. & Liu, X. Y. 1986. Paleoplate tectonics between Cathaysia and Angaraland in Inner Mongolia of China, *Tectonics* **5**, 1073–88.

Wang, H., Wang, Y. J., Chen, Z. Y., Li, Y. X., Su, M. R. & Bai, L. B. 2005. Discovery of the Permian radiolarians from the Bayanaobao area, Inner Mongolia. *Journal of Stratigraphy* **29**, 368–71.

Wang, T. Y., Wang, S. Z. & Wang, J. R. 1994. *The Formation and Evolution of Paleozoic Continental Crust in Alxa Region*. Lanzhou: Lanzhou University Press.

Wang, X. C., Wilde, S. A., Xu, B. & Pang, C. J. 2016. Origin of arc-like continental basalts: implications for deep-Earth fluid cycling and tectonic discrimination. *Lithos* **261**, 5–45.

Wang, T., Zheng, Y. D., Gehrels, G. E. & Mu, Z. G. 2001. Geochronological evidence for existence of South Mongolian microcontinent—a zircon U–Pb age of granitoid gneisses from the Yagan-Onch Hayrhan metamorphic core complex. *Chinese Science Bulletin* **46**, 2005–7.

Whitehouse, M. J. & Platt, J. P. 2003. Dating high-grade metamorphism constraints from rare-earth elements in zircon and garnet. *Contributions to Mineralogy and Petrology* **145**, 61–74.

Windley, B. F., Alexeiev, D. V., Xiao, W., Kröner, A. & Badarch, G. 2007. Tectonic models for accretion of the Central Asian Orogenic Belt. *Journal of the Geological Society, London* **164**, 31–47.

Wu, T. R., He, G. Q. & Zhang, C. 1998. On Paleozoic tectonics in the Alxa region. *Acta Geologica Sinica* **72**, 256–63.

Wu, S. J., Hu, J. M., Ren, M. H., Gong, W. B., Liu, Y. & Yan, J. Y. 2014. Petrography and zircon U–Pb isotopic study of the Bayanwulashan Complex: constrains on the Paleoproterozoic evolution of the Alxa Block, westernmost North China Craton. *Journal of Asian Earth Sciences* **94**, 226–39.

Xiao, W. J., Huang, B. C., Han, C. M., Sun, S. & Li, J. L. 2010. A review of the western part of the Altaids: a key to understanding the architecture of accretionary orogens. *Gondwana Research* **18**, 253–73.

Xiao, W. J., Windley, B. F., Hao, J. & Zhai, M. G. 2003. Accretion leading to collision and the Permian Solonker suture, Inner Mongolia, China: termination of the central Asian orogenic belt. *Tectonics* **22**, 1069.

Xiao, W. J., Windley, B. F., Huang, B. C., Han, C. M., Yuan, C., Chen, H. L., Sun, M., Sun, S. & Li, J. L. 2009. End-Permian to mid-Triassic termination of the accretionary processes of the southern Altaids: implications for the geodynamic evolution, Phanerozoic continental growth, and metallogeny of Central Asia. *International Journal of Earth Sciences* **98**, 1189–217.

Xiao, W. J., Windley, B. F., Sun, S., Li, J. L., Huang, B. C., Han, C. M., Yuan, C., Sun, M. & Chen, H. L. 2015. A tale of amalgamation of three Permo-Triassic collage systems in Central Asia: oroclines, sutures, and terminal accretion. *Annual Review of Earth and Planetary Sciences* **43**, 477–507.

Xie, L., Yin, H. Q., Zhou, H. R. & Zhang, W. J. 2014. Permian radiolarians from the Engeerwusu suture zone in Alxa area of Inner Mongolia and its geological significance. *Geological Bulletin of China* **33**, 691–7.

Xu, B., Charvet, J., Chen, Y., Zhao, P., Shi, G. Z. 2013. Middle Paleozoic convergent orogenic belts in western Inner Mongolia (China): framework, kinematics, geochronology and implications for tectonic evolution of the Central Asian Orogenic Belt. *Gondwana Research* **23**, 1342–64.

Xu, B., Zhao, P., Bao, Q. Z., Zhou, Y. H., Wang, Y. Y. & Luo, Z. W. 2014. Preliminary study on the pre-Mesozoic tectonic unit division of the Xing-Meng Orogenic Belt (XMOB). *Acta Petrologica Sinica* **30**, 1841–57 (in Chinese with English abstract).

Yang, Z. Y., Liu, H., Zhang, D. J., Li, X. & Sun, Y. W. 2015. Detrital zircon U–Pb dating of Upper Carboniferous–Lower Permian Amushan Formation in Bayan Obo area, Inner Mongolia and its geological implications. *Global Geology* **34**, 259–72.

Yang, J. H., Wu, F. Y., Shao, J. A., Wilde, S. A., Xie, L. W. & Liu, X. M. 2006. Constraints on the timing of uplift of the Yanshan Fold and Thrust Belt, North China. *Earth and Planetary Science Letters* **246**, 336–52.

Yuan, W. & Yang, Z. Y. 2015. The Alashan Terrane did not amalgamate with North China block by the Late Permian: evidence from Carboniferous and Permian paleomagnetic results. *Journal of Asian Earth Sciences* **104**, 145–59.

Zhang, Z. C., Chen, Y., Li, K., Li, J. F., Yang, J. F. & Qian, X. Y. 2017. Geochronology and geochemistry of Permian bimodal volcanic rocks from central Inner Mongolia, China: implications for the late Palaeozoic tectonic evolution of the south-eastern Central Asian Orogenic Belt. *Journal of Asian Earth Sciences* **135**, 370–89.

Zhang, S.-H., Li, Z. X., Evans, D. A. D., Wu, H. C., Li, H. Y. & Dong, J. 2012. Pre-Rodinia supercontinent Nuna shaping up: a global synthesis with new paleomagnetic results from North China. *Earth and Planetary Science Letters* **353–354**, 145–55.

Zhang, J., Li, J. Y., Xiao, W. X., Wang, Y. N. & Qi, W. H. 2013a. Kinematics and geochronology of multistage ductile deformation along the eastern Alxa block, NW China: new constraints on the relationship between the North China Plate and the Alxa block. *Journal of Structural Geology* **57**, 38–57.

Zhang, X. H., Mao, Q., Zhang, H. F., Zhai, M. G., Yang, Y. H. & Hu, Z. C. 2011. Mafic and felsic magma interaction during the construction of high-K calc-alkaline plutons within a metacratonic passive margin: the Early Permian Guyang batholiths from the northern North China Craton. *Lithos* **125**, 569–91.

Zhang, J. J., Wang, T., Zhang, L., Tong, Y., Zhang, Z. C., Shi, X. J., Guo, L., Huang, H., Yang, Q., Huang, W., Zhao, J. X., Ye, K. & Hou, J. Y. 2015. Tracking deep crust by zircon xenocrysts within igneous rocks from the northern Alxa, China: constraints on the southern boundary of the Central Asian Orogenic Belt. *Journal of Asian Earth Sciences* **108**, 150–69.

Zhang, W., Wu, T. R., Feng, J. C., Zheng, R. G. & He, Y. K. 2013b. Time constraints for the closing of the Paleo-Asian Ocean in the Northern Alxa Region: evidence from Wuliji granites. *Science China Earth Sciences* **56**, 153–64.

Zhang, Y. Q. & Zhang, T. 2016. Amushan Formation in Inner Mongolia. *Geology in China* **43**, 1000–15 (in Chinese with English abstract).

Zhang, Z., Zhang, H. F., Shao, J. A., Ying, J. F., Yang, Y. H. & Santosh, M. 2014*a*. Mantle upwelling during Permian to Triassic in the northern margin of the North China Craton: constraints from southern Inner Mongolia. *Journal of Asian Earth Sciences* **79**, 112–29.

Zhang, X. H., Zhang, H. F., Tang, Y. J., Wilde, S. A. & Hu, Z. C. 2008. Geochemistry of Permian bimodal volcanic rocks from central Inner Mongolia, North China: implication for tectonic setting and Phanerozoic continental growth in Central Asian Orogenic Belt. *Chemical Geology* **249**, 262–81.

Zhang, X. R., Zhao, G. C., Eizenhöfer, P. R., Sun, M., Han, Y. G., Hou, W. Z., Liu, D. X., Wang, B., Liu, Q. & Xu, B. 2014b. Paleozoic magmatism and metamorphism in the Central Tianshan block revealed by U–Pb and Lu–Hf isotope studies of detrital zircons from the South Tianshan belt, NW China. *Lithos* **233**, 193–208.

Zhang, S.-H., Zhao, Y., Kröner, A., Liu, X.-M., Xie, L.-W. & Chen, F.-K. 2009a. Early Permian plutons from the northern North China Block: constraints on continental arc evolution and convergent margin magmatism related to the Central Asian Orogenic Belt. *International Journal of Earth Sciences* **98**, 1441–67.

Zhang, S.-H., Zhao, Y., Song, B., Hu, J.-M., Liu, S.-W., Yang, Y.-H., Chen, F.-K., Liu, X.-M. & Liu, J. 2009b. Contrasting Late Carboniferous and Late Permian–Middle Triassic intrusive belts from the northern margin of the North China block: geochronology, petrogenesis and tectonic implications. *Geological Society of America Bulletin* **120**, 181–200.

Zhang, S. H., Zhao, Y., Yang, Z. Y., He, Z. F. & Wu, H. 2009c. The 1.35 Ga diabase sills from the northern North China Craton: implications for breakup of the Columbia (Nuna) supercontinent. *Earth and Planetary Science Letters* **288**, 588–600.

Zhang, S. H., Zhao, Y., Ye, H., Liu, J. M. & Hu, C. Z. 2014c. Origin and evolution of the Bainaimiao arc belt: implications for crustal growth in the Southern Central Asian Orogenic Belt. *Geological Society of America Bulletin* **126**, 1275–300.

Zheng, R. G., Wu, T. R., Zhang, W., Xu, C., Meng, Q. P. & Zhang, Z. Y. 2014. Late Paleozoic subduction system in the northern margin of the Alxa block, Altaids: geochronological and geochemical evidences from ophiolites. *Gondwana Research* **25**, 842–58.

Zhou, Y. Z., Han, B. F., Xu, Z., Ren, R. & Su, L. 2013. The age of the Proterozoic rocks in Yingba area in western Inner Mongolia: constraints on the distribution of the South Gobi micro-continent in the Central Asian orogenic belt. *Geological Bulletin of China* **32**, 318–26.

https://doi.org/10.1017/S0016756817000978 Published online by Cambridge University Press